2010:030 PB

MASTER'S THESIS

Standing Contact Fatigue Analysis of Steels with Different Microstructures

Ranga Naveen Kumar

M.Sc. in Advanced material Science and Engineering
CONTINUATION COURSES

Department of Applied Physics and Mechanical Engineering
Division of Engineering Materials

2010:030 PB • ISSN: 1653 - 0187 • ISRN: LTU - PB - EX - - 10/030 - - SE

MASTER'S THESIS

Standing Contact Fatigue Analysis Of Steels with Different Microstructures

RANGA NAVEEN KUMAR

EUROPEAN MASTER PROGRAMME IN ADVANCED MATERIALS SCIENCE AND ENGINEERING (AMASE)

Luleå University of Technology
Department of Applied Physics and Mechanical Engineering
Division of Engineering Materials

Abstract

High performance steels has been studied in this master thesis. The main objective was to understand the contact fatigue resistance of one silicon containing steel which can be treated in order to give it a carbide free bainitic microstructure.

Different microstructures of the steels were produced by austenitizing followed by different cooling cycles as austempering processes with which microstructures with high strength, good ductility, high toughness and excellent wear resistance can be achieved.

The work is divided into three-main parts. The first part treats the production of different micro structure as austenitic-ferritic structure, fully pearlitic, fully martensitic, quenched & tempered and lower bainitic structure respectively, including metallographic observations.

The second part treats the special Standing Contact Fatigue (SCF) analysis used in the work, which consists of cyclic loading of a hard ball in contact with the flat surface of the specimen, which is meant to simulate asperity contact in surface contact fatigue analysis.

The third part deals with the characterization and analysis of the results obtained for the ausferritic and the other microstructure in the work.

The experimental results have shown that the ausferritic structure has a very good combination of material properties like good contact fatigue resistance, high strength, ductility and toughness properties.

The microstructure before and after the tests were analyzed with the help of Optical microscopy, SEM microscopy, XRD analysis and additional analysis was performed by micro hardness measurements.

List of figures

List of tables

Appendix

Acknowledgment

The most important achievement in succeeding my master theis work is the guidance and support I received from my advisor, Esa Vuorinen. I have learned immensely from him. He taught me how to find direction in thesis work, drill down to the essentials, and make a dissertation out of it. I am highly grateful to him for making my thesis work such a smooth and rewarding experience.

Also, of importance to this work is the supportive environment I found at Department of Applied Physics and Mechanical Engineering lab, where I worked until the end of October 2009. I appreciate my colleague's interest in my work and their morale support, for which I would like to thank them very much. In particular, the creative atmosphere in the Division of Engineering Materials group, originally with Johnny Grahn, and later with Lennart Wallström supported my ascent to prevail on top of this dissertation. I wish to thank them all.

I have collaborated with many people over the last years, and in one way or another, they have influenced my thinking. Of particular importance to me are the discussions I had with Anusha Kankanala and Syed Abdul Khadar I would like to thank them very much. In a similar vein, I would like to thank Mathias Linz for his kind support.

Content

1. Background

Failure of structural materials under cyclic application of stress or strain is not only a subject of technical interest but one of industrial importance as well. The understanding of fatigue mechanisms (damage) and the development of constitutive equations for damage evolution leading to crack initiation and propagation as a function of loading history represent a fundamental problem for scientists and engineers.

The process of fatigue cracking generally begins from locations where there are discontinuities or where plastic strain accumulates preferentially in the form of slip bands. In most situations, fatigue failures initiate in regions of stress concentration such as sharp notches, nonmetallic inclusions, or at preexisting crack-like defects. When failures occur at sharp notches or other stress raisers, cracks first initiate, then propagate to critical size, and then failure occurs [1].

Contact fatigue damage may develop in surfaces subjected to repeated rolling and sliding contact, e.g. gear flanks and bearing surfaces. The end result is small craters in the contacting surfaces, named `spalls' by Tallian [2].

There are many causes and forms of fracture, and careful analysis of fractured parts requires an understanding of the component design, service loading, environments, and structure-property relationships. Knowledge of sound laboratory techniques in materials, and the examination and interpretation of fracture surfaces is very much required.

The work presented here adds to the understanding of why contact fatigue cracks has developed, which when considered in the design process will lead to simplified design work, reduction of extensive test series and improved contact fatigue resistance of applications.

1.1 Introduction

The test procedure named Standing Contact Fatigue (SCF) is used for surface initiated contact fatigue studies and the contact fatigue damage is mainly created by tensile surface stresses of the material. The contact fatigue cracks follows the same rules as ordinary fatigue cracks in hardened steel.

The majority of microcracks are arrested at a shallow angle to the surface, but some may continue to propagate parallel to the surface creating a macro scale fatigue crack. Several experimental methods have been developed in order to simulate the application conditions, including control of numerous influencing parameters [3].

The failure process can be divided into three phases: 1) a brief initial phase of bulk changes in the material, 2) a long, stable phase when only micro-scale changes take place and 3) the final phase when a macro-crack grows. During the first phase, bulk changes in the material structure occur in the highly stressed volume under the contact path. In the second phase, deformation bands, described as white etching areas, are created by the micro-plastic flow.

When this deformation bands are created around a defect such as an inclusion or an asperity they may be designated as butterflies. Sometime during this stable phase, micro-cracks are initiated at defect locations within the plastically deformed material. The microcracks usually occur at the contact surface or at the depth of maximum Hertzian shear stress. When numerous micro-cracks initiate at the surface the phase is named surface distress. See Figure 1.Surface distress is the result of the two first phases in the contact failure process.

Figure 1. Surface Distress.

The micro-crack, which is developed due to high hertzian stresses, propagates down into the material up to the maximum hertzian shear stress level, and then the crack turns into a surface parallel direction e.g. 1. In railway tracks the crack branches down to a steep angle against the surface causing the railway track to failure. 2. In bearing and gear applications the macro crack branches upward to the free surface. [4]

High performance rail steels or gear materials must have good fatigue resistance and at the same time high level of hardness and tensile strength. A rule of thumb often quoted is that the fatigue strength of ferrous materials is approximately one half of the tensile strength. Therefore strength of the material has been increased in this work by performing austempering treatment and was beneficial for fatigue resistance.

In this work the main aim was to do a careful investigation on contact fatigue resistance of a silicon alloyed bainitic steels with an austenitic-ferritic carbide free microstructure in comparison to the same steel with fully pearlitic and fully martensitic microstructure and also a comparison to a quench & tempered SS14 – 2244 which has been tempered at 200°C for 1 hr and at ca 550°C for 1 hr respectively and finally heat treated in order to achieve a lower bainitic microstructure by austempering at suitable temperatures.

2. Theory

2.1 Fatigue Properties

Fatigue cracking is one of the major and primary damage mechanics in structural components. The basic definition of "fatigue" is based on the concept that a material becomes "tired" and fails at a stress level below the nominal strength of the material. The cracking can result from cyclic stress below the ultimate tensile stress, or even the yield stress of the material.

When a sufficiently high load is applied to a metal or other structural material, it will cause the material to change shape. This change in shape is called deformation. If the material comes back to its original shape after removing the load than the property of the material is said as an elastic property. This type of deformation involves stretching of the atomic bonds. If the load or stress levels are increased than the bonds between the atoms break down and the material reach to a plastic deformation region by the movement of the dislocations.

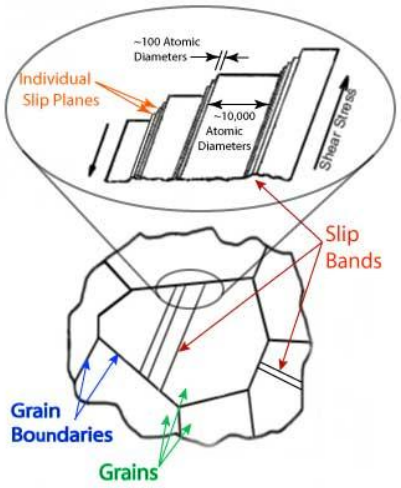

Figure 2. Slip bands in a material [5].

When high loads are applied the dislocations in the material have a preferred direction of travel within a grain of the material. This results in slip that occurs along parallel planes within the grain. These parallel slip planes group together to form slip

bands, which can be seen with an optical microscope. A slip band appears as a single line under the microscope, but it is in fact made up of closely spaced parallel slip planes as shown in the Figure 2.

The fatigue life can be defined as the number of cycles required to initiate and propagate a crack to its critical stage. Fatigue occurs mainly in 3 - stages

1. Crack formation and initiation which is a slow process. The dislocations play a major role in the crack initiation phase. They accumulate mostly near surface stress concentrations and form a structure called persistent slip bands (PSB) after undergoing a large number of cycles. Due to movement of material along the slip planes it leaves tiny steps in the surface that can serve as a stress risers and this can initiate a crack in the material. These cracks are called micro-cracks.

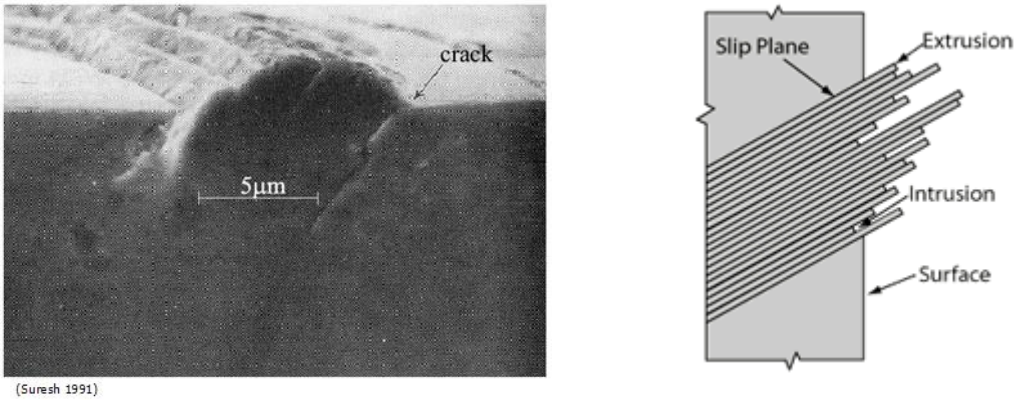

Figure 3. (a) Persistent slip bands (b) Dislocation fatigue in a material [5].

2. Stable crack growth. In this stage some of the micro cracks join together and begin to propagate through the material in a direction perpendicular to applied maximum tensile stress or load. Eventually, with continuous cyclic loading the larger cracks grow and dominate the material due to which the component can no longer support the load.

3. Rapid crack growth leading to fracture of a material. At this point, the fracture toughness is exceeded and the material experiences a rapid fracture.

2.2 Factors Affecting Fatigue Life

Basic factors affecting the fatigue life and crack initiation are, first of all the loading pattern that must contain minimum and maximum peaks, which can be in tension or compression with large enough variation or fluctuation for the crack to be initiated in the material. Secondly, the peak stress levels must be high enough. If the peak stresses are too low, no crack initiation will occur in the specimen. Thirdly, the material must experience a sufficiently large number of cycles of the applied stress.

The other variables which can affect the fatigue life and its properties are [5]

1. Mechanical properties of the material
2. Loading conditions
3. Stress concentrations
4. Corrosion
5. Overload
6. Residual stresses
7. Temperature
8. Notches & Scratches
9. Metallurgical structure
10. Surface condition of the specimen.
11. Surface roughness.
12. Compressive residual stress from heat treatments and machining can oppose a tensile load and thus lower the amplitude of cyclic loading.

2.3 Mechanical properties and its influence on fatigue life

The most common mechanical properties which are used in order to classify and identify materials are strength, ductility, hardness, impact resistance, and fracture toughness. These properties involve a reaction to applied loads. Structural materials are mostly un-isotropic and a material property varies with the orientation. One reason for the variation in properties of a material can be due to the directionality of the microstructure (texture) formed during the manufacturing processing of the material.

Ductility is used as a quality control measure to know the impurities and proper processing of a material. It is defined as measure of the extent to which a material will deform before fracture.

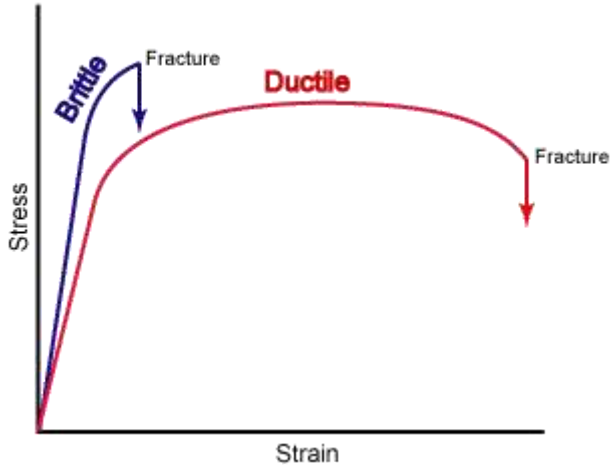

Figure 4. Stress-strain curve for brittle & ductile material [5].

The conventional measures of ductility are the engineering strain at fracture (usually called the elongation) and the reduction of area at fracture.

Hardness is defined as resistance of a material to localized deformation. The hardness is not considered as a basic property of a material, but rather a composite one with contributions from the yield strength, work hardening, true tensile strength, modulus, and others factors. The hardness measurements is very quick and considered as non destructive testing of materials when the marks or indentations produced by the test are in low stress areas and widely used for the quality control of the material.

Toughness is defined as the ability of a metal to absorb energy during the deformation process before fracture. A good ductile material does not become a tough material. A combination of good strength and ductility leads to toughness. A material which shows high strength and high ductility will have higher toughness than a material having low strength and high ductility.

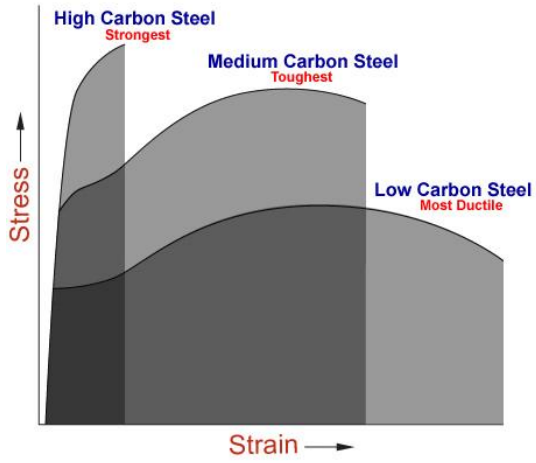

Figure 5. Toughness curve of a material [5].

So, the best way of calculating the toughness of a material is to calculate the area under the stress-strain curve from a tensile test as shown in Figure 5. The unit of toughness is energy per volume. The toughness is influenced by the following variables.

- Rate of loading (Strain rate)
- Temperature
- Geometrical (Notch) effect

A metal can fail due to cyclic or dynamic loading conditions, but may possess satisfactory toughness results under static loads and therefore it can be said that the toughness of a material decreases with increase in loading and vice versa.

Tension, compression, bending, shear, and torsion are the five-basic and fundamental loading conditions that can be applied to a material. In this thesis work the loading of the material is not constant but instead fluctuating.

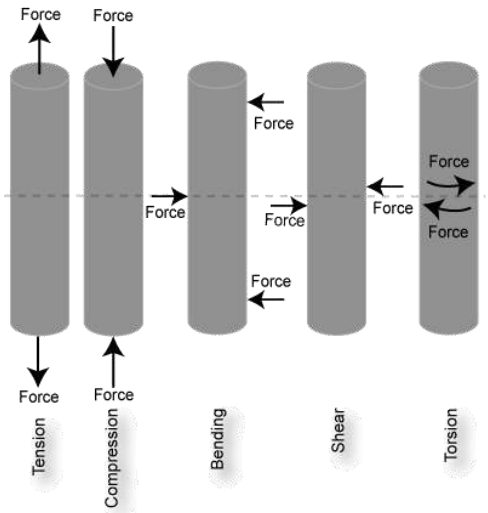

Figure 6. The different loading modes in most common material [5].

The way in which the material is loaded will greatly affect its mechanical properties and largely determines how, or if, a component will fail; and whether it will show warning signs before failure actually occurs.

Tensile strength is one important property of the material in analyzing the fatigue failure. Tensile strength is correlated to hardness. This correlation depends upon specific test data and cannot be extrapolated to include other materials not tested.

$$\text{TS (MPa)} = \begin{cases} 3.55 \cdot HB & (HB \leq 175) \\ 3.38 \cdot HB & (HB > 175) \end{cases}$$

$$\text{TS (psi)} = \begin{cases} 515 \cdot HB & (HB \leq 175) \\ 490 \cdot HB & (HB > 175) \end{cases}$$

For a material with good yield strength values it is always difficult for the cracks to initiate and propagate as it is in relation with the hardness of the material.

2.4 Stress Life Fatigue Analysis

The Stress-Life method (also referred to as the S-N method) is used to understand and quantify the metal fatigue. The Stress-Life method does not work well in low-cycle applications, where the applied strains have a significant plastic component due to high load levels. Roughly speaking, low-cycle fatigue applications are those with less than 10,000 loading cycles during the component life and High-cycle fatigue is associated with component lives greater than 100,000 cycles. The transition life between low- and high-cycle fatigues depends on the material being considered, and is usually between 10,000 and 100,000 cycles. In general, the Stress-Life approach should not be used to estimate fatigue lives below 10,000 cycles.

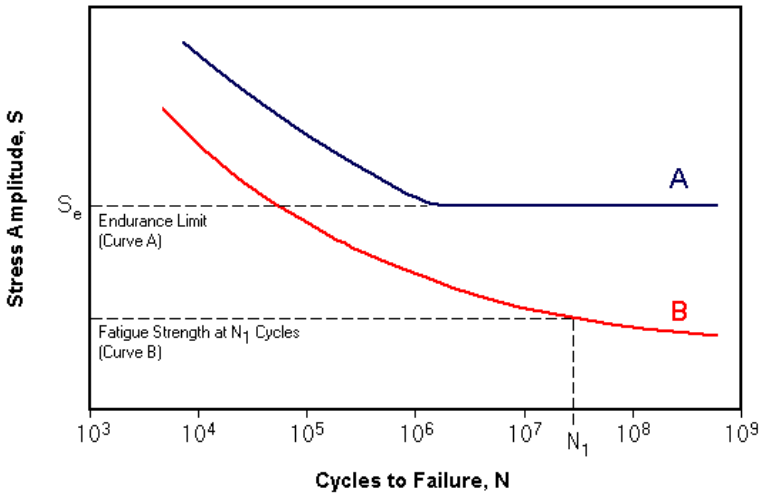

Figure 7. Typical amplitude vs. failure cycles curve (S-N curve).

The S-N diagram plots nominal stress amplitude (S) versus number of cycles to failure (N) see Figure 7. The S-N test data are usually displayed on a log-log plot, with the actual S-N line representing the mean of the data from several tests. There are some materials which have a fatigue limit or endurance limit which represents a stress level below which the material does not fail and can be cycled infinitely i.e. material is having an infinite life. The endurance limit is not a true property of a material, since other significant influences such as surface finish cannot be entirely eliminated. Influences that can affect the endurance limit include:

- Surface Finish
- Temperature
- Stress Concentration
- Notch Sensitivity
- Size
- Environment
- Reliability

Steels and Titanium alloys Curve-A in Figure 7 show endurance limit and there are non ferrous materials with face centered cubic lattice structures like Aluminum and Copper alloys which show no endurance limits as shown in Figure 7 the B-red curve line.

The usual procedure is to test the first specimen at a high peak stress where failure is expected in a fairly short number of cycles. The test stress is decreased for each succeeding specimen until one or two specimens do not fail for specified numbers of cycles. The fatigue limit for the steel material is 35 – 60 % of the tensile strength. The interstitial elements like carbon and nitrogen in iron play a vital role in preventing the slip mechanism which leads to formation of micro-cracks [6]. Care must be taken when using an endurance limit in design applications because it can disappear due to:

- Periodic overloads (unpin dislocations)
- Corrosive environments (due to fatigue corrosion interaction)
- High temperatures (mobilize dislocations)

2.5 Types of Cracks in a SCF – Test

The Standing Contact Fatigue (SCF) experiment shows that a local contact can produce sufficiently large tensile radial stresses to create surface fatigue cracks. If the total load and number of cycles required to initiate a crack are above the fatigue level than the fatigue cracks are developed. The 4 - different types of cracks that can develop during the cyclic loading of SCF test rig are

1. Ring / cone Crack
2. Lateral crack
3. Median crack
4. Radial crack.

1. Ring / Cone Crack :

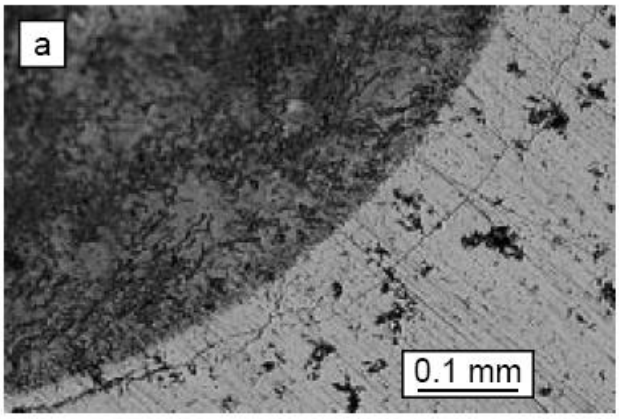

Figure 8. Top view of ring / cone Crack.

This type of ring cone crack is produced if the total load is above the endurance limit level. The ring/cone cracks are normally formed at, or up to 17% outside the cyclic contact radius. The distance between the contact rim and the crack increases with external load level. The cracks are initially perpendicular to the surface, and as they propagate into the material they turn outward forming truncated cones. The crack angle β to the surface at the crack front decreases with crack length as is illustrated in Figure 9.

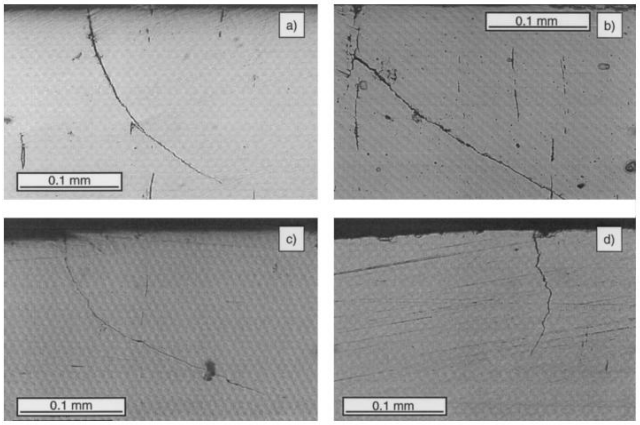

Figure 9. Detailed cut views of Ring / Cone Crack with load 16 KN, N = (110, 110, 112, 60)10^3 cycles, β = 26, 28, 21, 90^0 and s = (0.23, 0.35, 0.27, 0.13) mm for the cracks in (a)-(d), respectively.

Figure 9 shows the Detailed cut views of four ring/cone cracks when the load is 16 KN, No of cycles N= (110, 110, 112, 60) * 10^3 cycles, Angle of crack β= (26, 28, 21, 90) ^{0} and Length of the crack s = (0.23, 0.35, 0.27, 0.13) mm (a)-(d), respectively [11].

2 Lateral Crack :

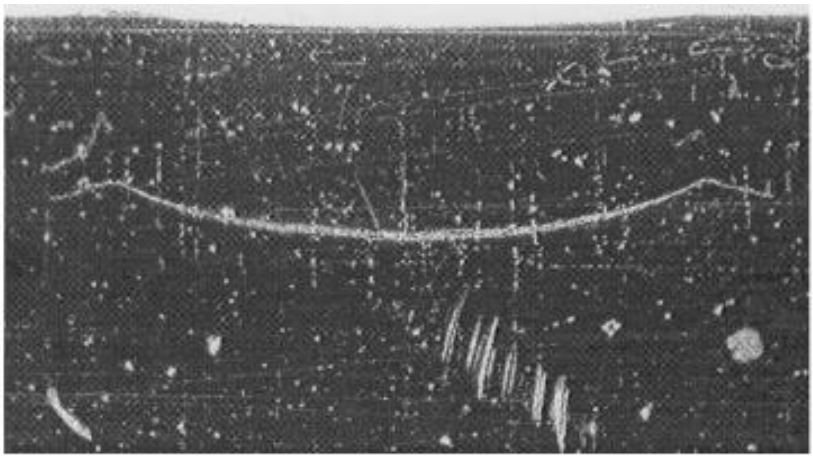

Figure 10. Lateral crack cut view.

The mechanism behind the SCF lateral crack is found to be important in order to understand the sub-surface initiated spalling damage. It is developed below the contact surface after some repeated cyclic number of loads. With increase in external total load the overall length of crack also increases. From Figure 10 we get information about the lateral cracks showing the characteristic shallow U-shape .Approximately it is seen at a

depth of z = 0.65mm from the surface [11]. The crack defection angle may be ranged between 36 º – 50 º. Figure 14 shows us the cracks which can develop during an SCF test.

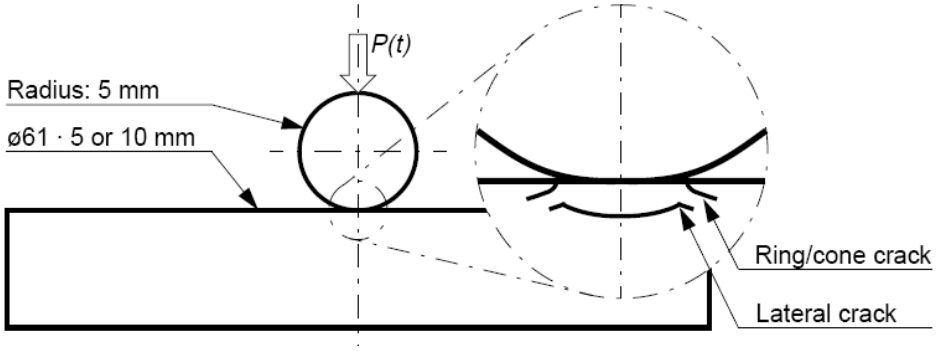

Figure 11. SCF set-up with Ring / Cone and Lateral Crack [11].

3 Median Crack :

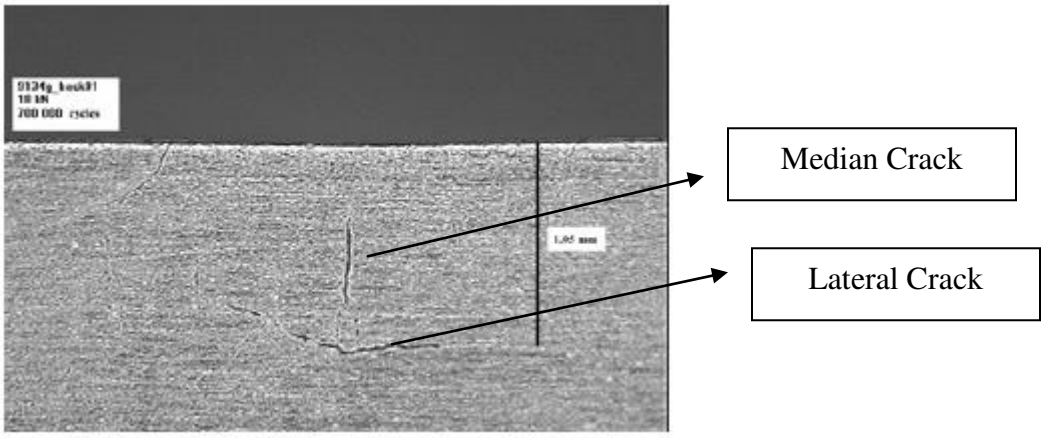

Figure 12. Lateral and median cracks formed during SCF test.

Median cracks are found between the lateral crack and the contact surface. Median crack normally starts at or near the lateral crack and extends towards the external surface as shown in Figure 12. No median cracks have been identified in SCF test without lateral cracks. The median crack is therefore a result of the redistributed stress state occurring when a lateral crack is present [11].

4 Radial Crack :

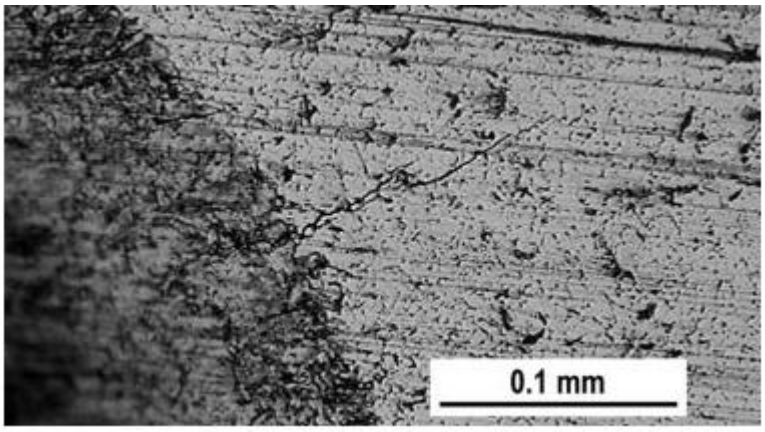

Figure 13. Radial crack formed during SCF test.

Radial Crack may develop from a tensile hoop stress, which is present only after substantial plastic deformation as shown in Figure 10. In the elastic range the surface hoop stress is compressive. The radial crack extends in the radial direction from the contact rim and travels outwards as seen in Figure 13 [7].

2.6 Surface Hardened Steel

In order to be able to give a comparison on the work done by Mathias Linz in the discussion part the contact fatigue resistance of bainitic-ferritic microstructure is compared with the heat treated surface hardened steel. Surface hardening is a process used to improve the wear resistance of parts without affecting the softer, tough interior of the part.

For the surface-hardened steel which followed Swedish Standard 2506 the case hardness was 750 HV while the core remained at 450 HV. The yield strength, deformation hardening, residual stresses and fatigue properties were all affected by the surface hardening process and, thus, functions of the depth below the surface.

The material properties of the case and core were determined in separate tension tests, with the flow stress of the surface material well described by [11]

$$\sigma_{\mathrm{f,case}}(\varepsilon_{\mathrm{pl}}) = \sigma_{\mathrm{Y,\ case}} + H \cdot \varepsilon_{\mathrm{pl}}$$

Whereas the core material exhibit a non-linear relation as

$$\sigma_{\mathrm{f,core}}(\varepsilon_{\mathrm{pl}}) = \sigma_{\mathrm{Y,\ core}}\left(1 + \frac{\varepsilon_{\mathrm{pl}}}{\varepsilon_0}\right)^n.$$

At an arbitrary depth, the flow stress was assumed to follow linearly with the transformation strain.

$$\sigma_{\mathrm{f}}(\varepsilon_{\mathrm{pl}},z)=\sigma_{\mathrm{f,case}}(\varepsilon_{\mathrm{pl}})\cdot\left(\frac{\varepsilon_{\mathrm{t}}(z)}{\varepsilon_{\mathrm{t,case}}}\right)+\sigma_{\mathrm{f,core}}(\varepsilon_{\mathrm{pl}})\cdot\left(1-\frac{\varepsilon_{\mathrm{t}}(z)}{\varepsilon_{\mathrm{t,case}}}\right).$$

σ_f = Flow stress
σ_y = Yield stress
ε_t = Transformation strain
ε_{pl} = Effective Plastic strain
ε_o = Reference strain
n = Power law component
Z = Arbitrary depth
H = Linear Hardening Modulus

The test should serve as a direct way to compare the relative resistance to surface contact fatigue initiation of different materials.

3. Experimental Procedure

3.1 Standing Contact Fatigue (SCF)

A number of 'rolling contact fatigue' (RCF) tests have been developed in order to simulate the complete damage process. However, if focus is placed on investigating the physical mechanism of contact fatigue crack initiation, then the large number of parameters becomes a disadvantage. Therefore, the Standing Contact Fatigue (SCF) test has recently been developed [3]. Figure 14 show that a local point-type contact alone, such as for instance an asperity, can produce cracks in case hardened steel used for contact applications [7].

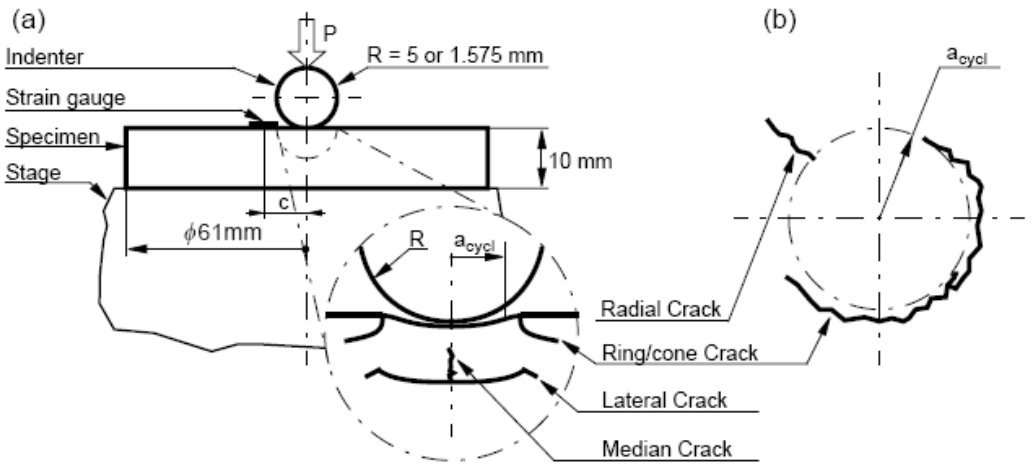

Figure 14 .The test rig and crack pattern (a) A side view (b) An enlarged top view [3].

The macro-cracks produced by the Standing Contact Fatigue (SCF) test and the micro-cracks produced by the Rolling Contact Fatigue (RCF) test finds a close relationship between them and indicates that these are created by similar mechanisms and supports an asperity based model [8].

The advantage with SCF test method is that it has some adjustable parameters, which makes it easier to interpret in between the fatigue results. Parameters that can be alternated are load, cycles, geometry and another advantage of this traditional experimental method is that they closely simulate the actual application conditions.

In order to achieve as pure normal contact as possible, steel material is chosen for both sphere and specimen. Here, the contact fatigue resistance of the specimen mainly depends upon the material hardness (resistance to indentations) Figure 15 shows the contact fatigue resistance for different materials.

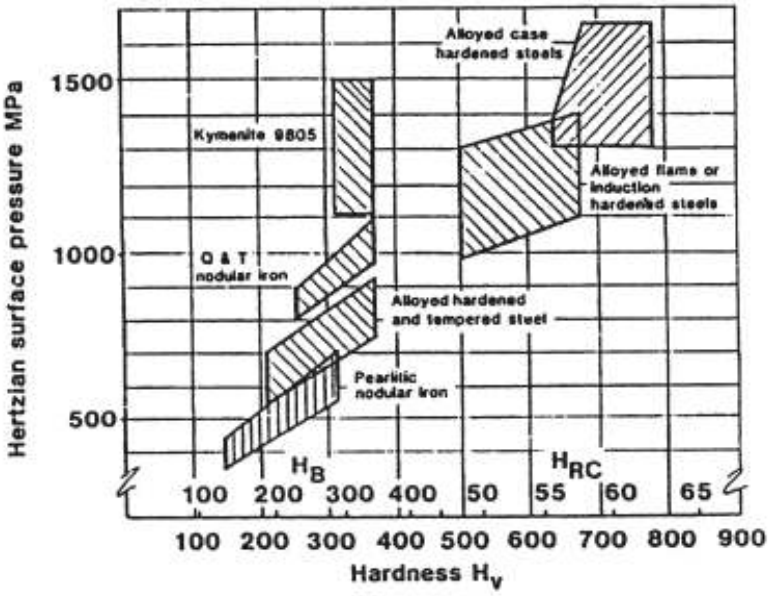

Figure 15. The Contact fatigue resistance for different materials as a function of hardness [9].

The indenter is stationary and loaded with a pulsating contact load. The load was cycled from 11 KN to 15 KN. The minimum compressive load of 0.5 KN was set to avoid loss of contact between specimen and indenter during the tests. All tests were stopped at predefined number of cycles, which varied between 33 000 to 70, 00,000 cycles.

All tests were performed without any lubrication. Crack initiation and propagation are therefore independent of mechanisms such as the “entrapped fluid mechanism”. Another parameter that is not involved in this test is the slip ratio between the contacts, which is a frequently used parameter in rolling contact fatigue. It is however possible to include slip in this type of test by tilting the supporting plane. Furthermore, no damage at the surfaces has been detected here in these current experiments that indicate the presence of fretting fatigue damage.

Theory

Fracture Mechanics of a Crack

Due to pulsating contact load between the indentator and the specimen different types of cracks can develop during the SCF test. The crack undermines the surrounding material through propagation and finally it causes a surface damage.

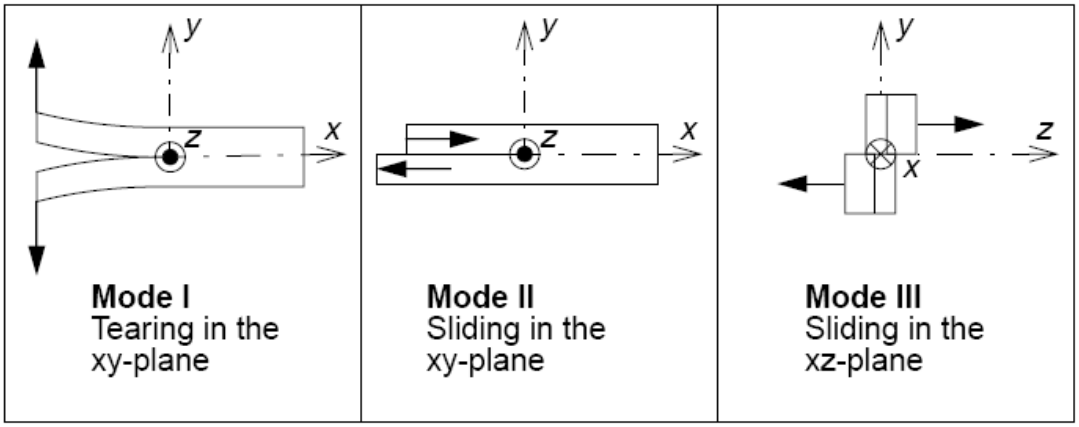

Figure 16. Fracture mechanics with different modes of a crack.

Fracture mechanics are used to model the macro-crack propagation phase. Linear Elastic Fracture Mechanics (LEFM) may be used if the relative size of the plastic zone at the crack-tip is small compared to the structure. If the structure (applied) load is known than there is a chance of getting information about the critical crack length, growth rate and direction of growth. In general Figure 16 shows us a crack tip which can be subjected to three types of loads, or modes [10].

4. Sample Preparation

The Standing contact fatigue SCF tests were carried out on circular discs of 10 mm thickness and diameter of 60 mm. For each specimen one side was prepared for the test by grinding (2500 grid) and polishing (upto 1 micrometer). The preparation enabled the fatigue cracks to be observed easily when the indents were inspected.

4.1 Metallographic Examination and Hardness Tests

Micro structural observations were made on the specimens. A metallographic finish was obtained by using the following procedure.

1. The BUEHLER grinder/polisher was used to prepare the specimens. Specimens were first ground using 60 to 1200 silicon carbide papers for few minutes depending upon the material to be removed and at each time the specimens were lubricated with running water.
2. The samples were then cleaned in an ultrasonic bath for 2 minutes.
3. The polishing stage started with the 9-micron ultra pad cloth and finished using the 1-micron Texmet cloth. Each polishing step was carried out with the appropriate diamond suspension.
4. A nital etch was used to reveal the microstructure.
5. Specimens were then examined in an OLYMPUS-BX60M optical microscope. A stereo zoom microscope type OLYMPUS SZ-CTV was also used to examine surface features such as surface fatigue test pits and micro pits. Micrographs from either microscope were obtained with a JVC camera type KY F55B to a computer loaded with a digital image processor (MARS).
6. Micro indentation hardness measurements were made using a Matzusawa Vickers Micro hardness tester with a load of 300g.

5. Experimental materials and methods used

The SCF experimental test procedure was carried on different microstructures of steel and the contact fatigue resistance of a material i.e. the fatigue limit (endurance limit) was obtained. Two alloys were used in this work to produce different microstructures; the chemical compositions are listed in Table 1. The materials were produced by Ovako steel company.

Table 1. Chemical composition used for producing different microstructures.

Alloy	Grade	C %	Si %	Mn %	Cr %	Mo %
A	60SiCr7 Steel	0.605	1.7	0.75	0.35	0.04
B	SS14 2244 Steel	0.42	0.25	0.75	1.05	0.2

Before heat treatment the basic microstructure of the 60SiCr7 steel specimen was a pearlitic microstructure. Figure 17 shows the pearlite microstructure.

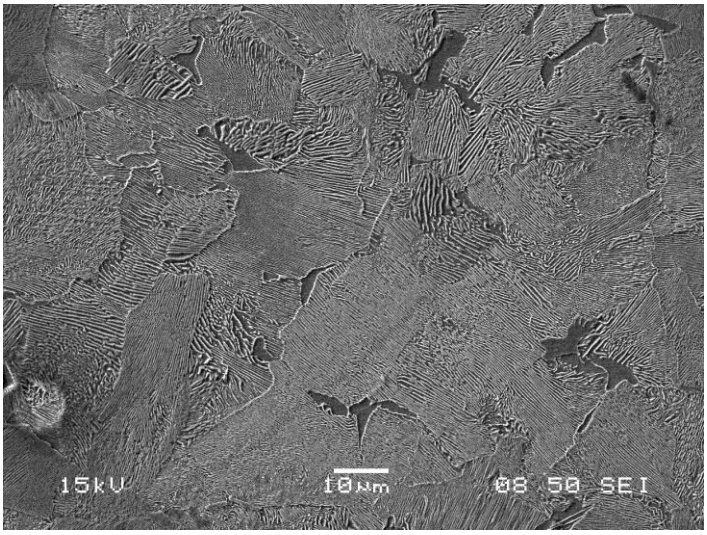

Figure 17. SEM image showing the pearlitic structure (before heat treatment) of 60SiCr7 steel specimen

5.1 Austenitizing / Cooling Procedure:

The test samples (1-7) shown in Table 2 were austenitized for 30 min at 850°C. Isothermal transformation was then carried out for specimens by quenching from the austenitization temperature into a salt bath at a preset temperature. The transformation was allowed in each case by keeping the samples in salt bath for 1 hour. Figure 18 shows the most common time-temperature isothermal transformation diagram for a steel material [13].

Table 2. Heat treatment of the experimental alloys.

Sno.	Alloy	Microstructure	Heat Treatment
1	A	Ausferritic Steel austempered at 250 ^{0}C	Austenized 850 ^{0}C for 30 hr , Isothermal at 250 ^{0}C for1 hr, Air cooled
2	A	Ausferritic Steel austempered at 275 ^{0}C	Austenized 850 ^{0}C for 30 hr , Isothermal at 275 ^{0}C for1 hr, Air cooled
3	A	Ausferritic Steel austempered at 300 ^{0}C	Austenized 850 ^{0}C for 30 hr , Isothermal at 300 ^{0}C for1 hr, Air cooled
4	A	Ausferritic Steel austempered at 350 ^{0}C	Austenized 850 ^{0}C for 30 hr , Isothermal at 350 ^{0}C for 1 hr, Air cooled
5	B	Lower bainite	Austenized 850 ^{0}C for 30 hr , Isothermal at 350 ^{0}C for 1 hr, Air cooled
6	B	Quench and Tempered (2244) (200 ^{0}C, 1 hr)	Tempered at 200 ^{0}C for 1 hr, Water cooled
7	B	Quench and Tempered (2244) Steel	Tempered at 550 ^{0}C for1 hr, Water cooled
8	A	Fully Pearlitic	Austenized 850 ^{0}C for 15 min, Isothermal 600 ^{0}C for 10 min, Air cooled
9	B	Fully Martensite	Austenized 850 ^{0}C for 1 hr, Isothermal 300 ^{0}C for10 min, Water cooled

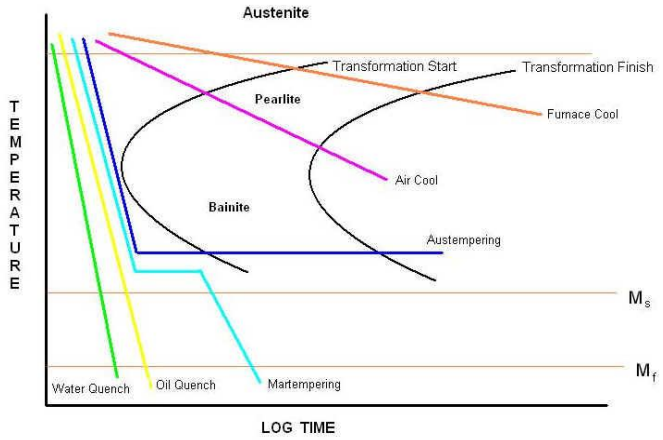

Figure 18. Time-temperature isothermal transformation diagram for steel material [13].

5.2 Fully Pearlitic microstructure:

Pearlitic microstructure was obtained by austenizing the steel specimens to a temperature of 850°C for 15 min and than hold down for 7 min near the furnace opening and followed by quenching the specimen in a salt bath to a temperature of 600°C for 10 min then air cooled. The average hardness value obtained for the pearlitic microstructure was355 HV.

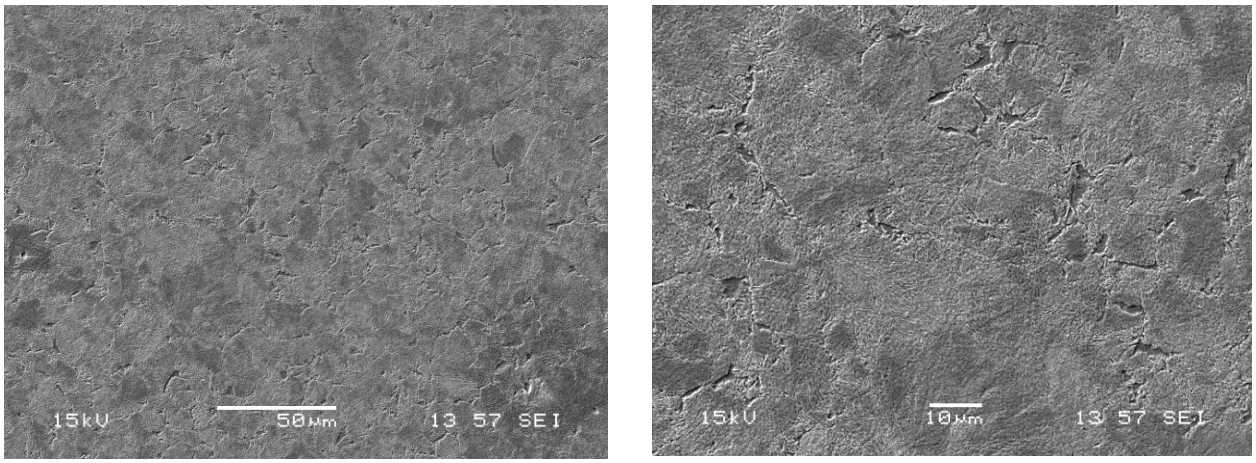

Figure 19. SEM images of Pearlitic structure.

5.3 Quenched & tempered microstructure (SS 14 2244 – steel):

Martensitic transformations are diffusion less. The change in crystal structure from FCC to BCT is achieved by homogeneous transformation of the parent phase .Martensite has lower density than the austenite and martensite transformation results in change of volume. With respect to different tempering temperature, there is a possibility of forming flakes or needles which consist of number of stress concentration areas. These areas can be reduced by the process tempering.

Figure 20. Needle structure of martensite [14].

The ductility and toughness can be increased by tempering process i.e. sacrificing hardness and brittleness. The treatment method is shown in Table 2. The tempering temperature will have significant effect on the material properties. The average hardness value obtained was 336 HV.

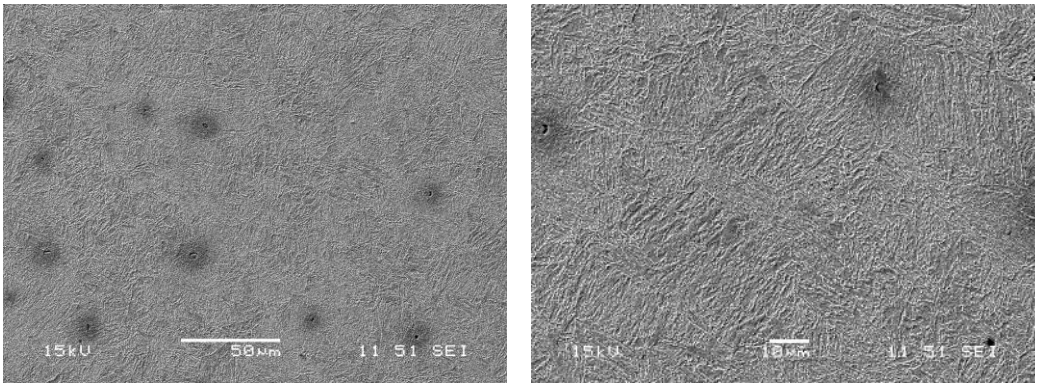

Figure 21. SEM images of Quenched and tempered (SS14 2244 Steel).

5.4 Lower bainitic microstructure:

Austempering is essentially an arrested quench process designed to produce a bainitic microstructure having properties that combine high hardness with toughness, resulting in a resistance to brittle fatigue. Austempering involves an isothermal transformation at a temperature below that of pearlite formation and above that of martensite formation as shown in Figure 22. The treatment method is shown in Table 2.

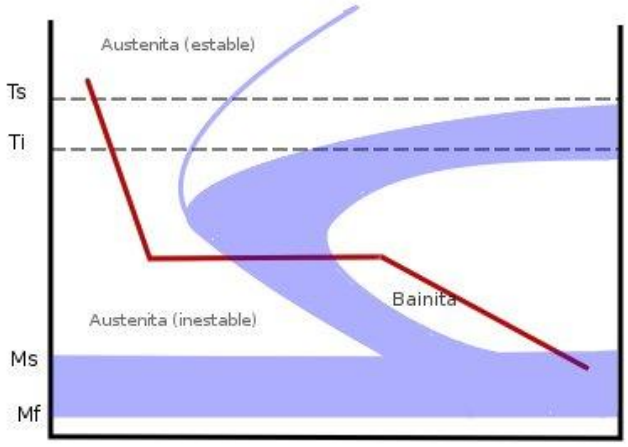

Figure 22. Austempering technique [15].

Austempering is a sometimes an overlooked process which offers great value where parts require a combination of high hardness and high toughness (ductility). Austempering is also of great benefit for parts requiring less heat treat distortion or dimensional variation and when breakage must be kept to a minimum. Lower bainitic steels are used in rails and gear manufacturing industries. The average hardness value for the lower bainitic structures obtained was 447 HV.

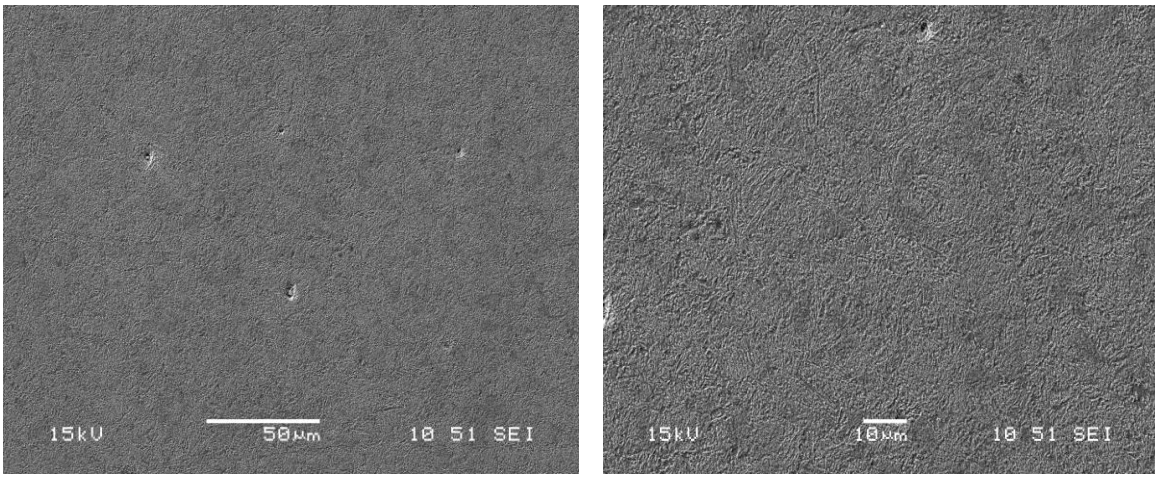

Figure 23. SEM images of lower bainite austempered at 350^{0}C.

5.5 Ausferritic microstructure:

A special microstructure called ausferritic microstructure is achieved by an austempering treatment in which the steel is cooled to a temperature above the Ms temperature. The treatment method is shown in Table 2. During this time ferrite will nucleate from the austenite and the amount of ferrite starts growing during the diffusion of carbon into the retained supersaturated austenite.

A schematic heat treatment cycle is shown in Figure 24. The specimen is heated to a temperature of 850 °C for 30 min. At this stage, the structure becomes fully austenitized and after austenitizing, the alloy is quenched in a molten salt bath and cooled to an austempering temperature range of between 250°C and 350°C. The specimen is maintained at this temperature range for about 1-2 hours depending upon requirement and then air cooled to room temperature.

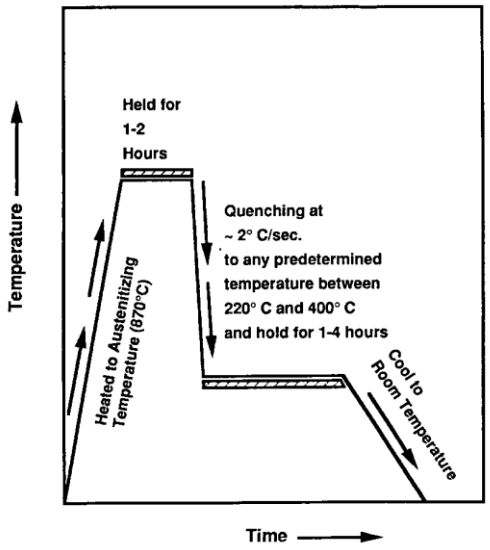

Figure 24. Heat Treatment Sequence for ausferritic Steel [16].

This structure, which is achieved by means of an austempering treatment and consisting of austenite and ferrite called ausferritic, is fine grained and free of carbides, presenting a good combination of properties such as high strength, good ductility and excellent wear resistance.

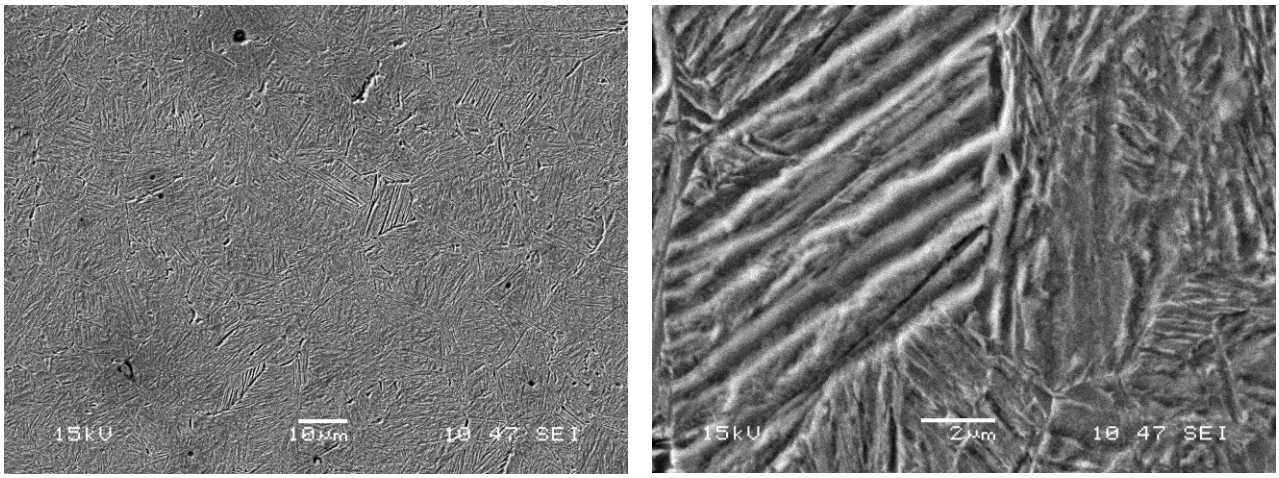

Figure 25. SEM images of a ausferritic steels austempered at 250^{0}C.

The potential advantages of such mixed microstructure can be listed as follows:

- Cementite is responsible for initiating fracture in high-strength steels. Its absence is expected to make the microstructure more resistant to failure.
- The microstructure obtained, looks like it is free of carbides and it derives its strength from the fine grain size of the ferrite plates.
- Steels with such type of microstructure can be obtained without the use of expensive alloying elements.

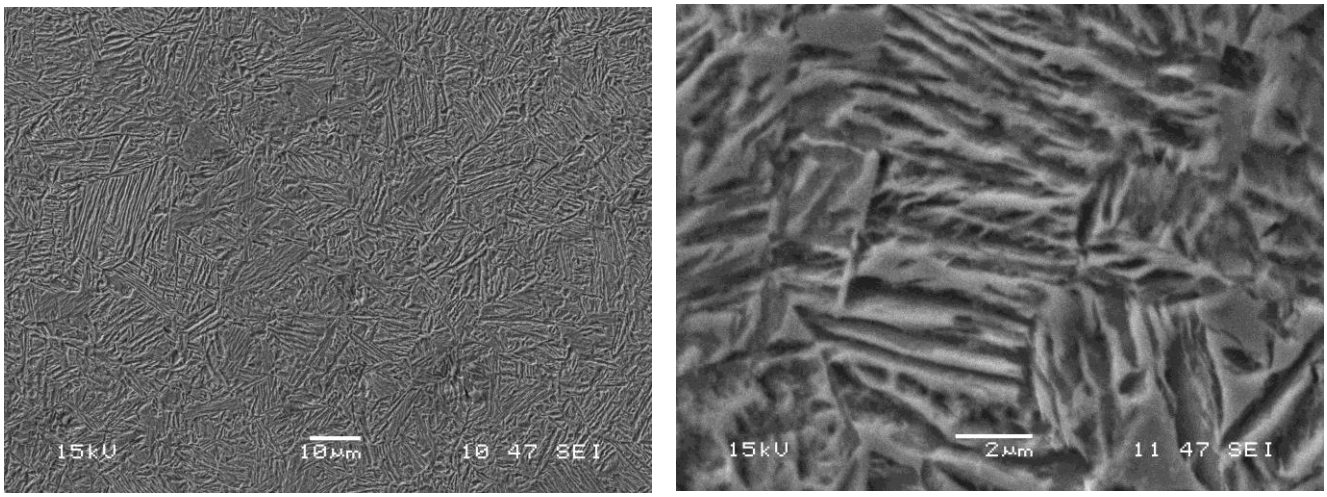

Figure 26. SEM images of Ausferritic steels Austempered at 350^{0}C.

5.6 Quench & tempered steel

Quench & tempered (SS 14 2244) steel was austenitized at a temperature of 850 °C for 1 hour and then the specimen was immersed in water having a temperature of 50 °C and then the sample was tempered at 200 °C for 1 hour in the salt bath followed by quenching in water which resulted in good strength and hardness of the material. The average hardness value obtained after the tempering was 532 HV.

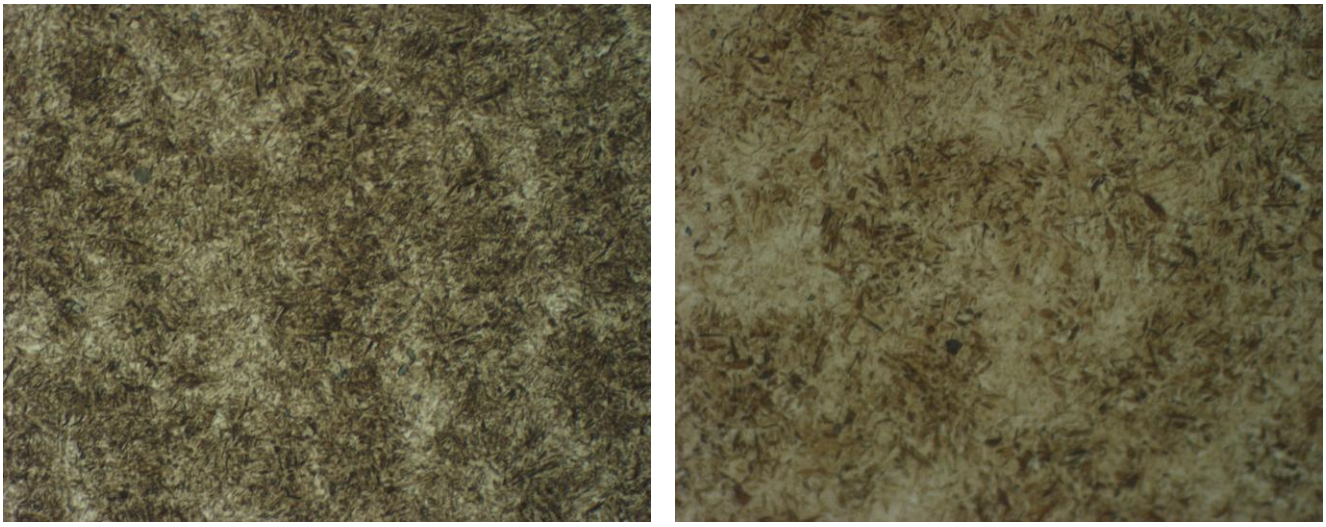

Figure 27. Optical microscope images of Quench and tempered (200 ºC, 1 hr) and fully Martensite specimens. 1000X

5.7 Fully martensitic structure:

The alloy - A was austenized to a temperature of 850 °C for 1 hour and then the transformation was allowed by keeping the samples in salt bath at a temperature of 300 °C for 10 min followed by quenching the sample into water which resulted in fully martensitic microstructure and the average hardness value resulted was 750 HV. Figure 27 shows the optical microscope image obtained after the heat treatment process.

6 Experimental equipments used

6.1 Scanning Electron Microscope

A schematic representation of the scanning electron microscope with which surfaces are studied is shown in Fig. 28. A narrow electron beam generated by an electron gun is focused down upon the sample by a system of electromagnetic lenses and apertures. The beam will not simply continue straight downwards through the sample, but get hit or scattered due to interactions with the sample's atoms which give rises to primary back scattered ,secondary and auger electrons. The volume of the sample into which the electrons penetrate is called the interaction volume and it is from this volume the signals used for visualization propagate.

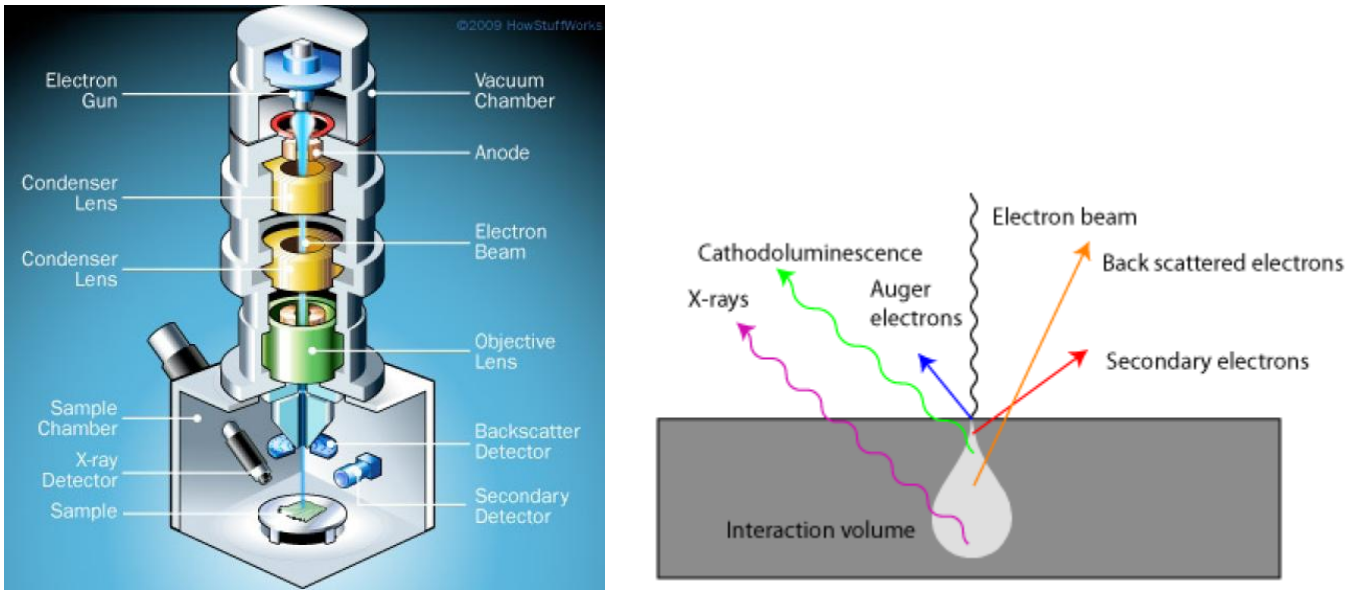

Figure 28. Scanning electron microscope and its working principle.

Electrons that interact strongly with the atoms of the sample will be ejected out of the sample surface with a minimum loss of energy and these are called backscattered electrons.

If the electrons are capable of transferring enough kinetic energy to the valence electrons of the sample atoms, these will be removed from the atoms and put in motion

and radiate outwards from the sample surface. This form of radiation is called secondary electrons and is characterized by the electrons having energy below 50 eV, which is less than the backscattered electrons.

The detectors present in the specimen chamber collects these electrons and convert them into useful information in the form of signals and sends to the display screen. The main advantages of owning a scanning electron microscope is the depth of field and the combination of higher magnification, larger depth of focus, greater resolution, and ease of sample observation makes the SEM one of the most heavily used instruments in research areas today.

6.2 Optical Microscope

The best optics in the world are useless if their alignment is wrong, or if they cannot be delicately adjusted to accommodate characteristics of the viewer and subject. These, and other non-optical requirements, are met by careful design to achieve the viewer's choice.

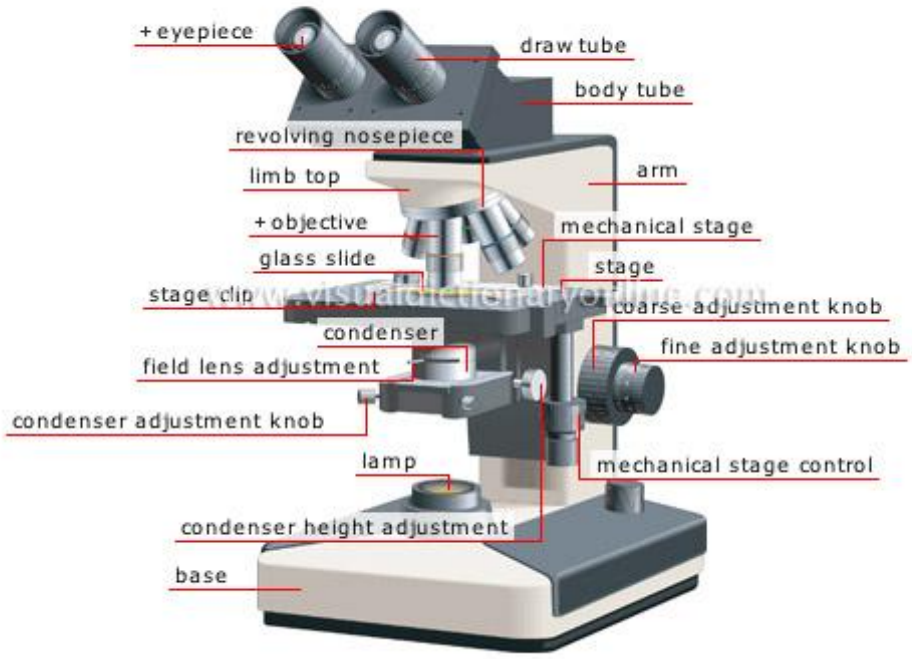

Figure 29. A schematic representation of the Optical Microscope.

The optical microscope components are its two imaging lenses (eyepiece and objective) and a condenser lens. The eyepiece and objective are responsible for magnifying the image of the specimen and projecting it onto the viewer's retina or onto the film plane in a camera and the job of the condenser lens is to focus a cone of incident

light onto the specimen. An illumination system or an external artificial light may direct towards the condenser lens. There is a movable stage which holds the specimen in the optical path and allows the specimen to be moved in and out of the focal plane and even left, right and rotated about the optic axis. The optical microscope may include other attachments like a camera, a viewing screen. The advantages of microscope are the technique is relatively inexpensive to set up and equally easy to use. Its reliability is unmatched and requires little or no sample preparation.

6.3 Vickers hardness testing machine

The hardness test machine uses a desk top machine. The Vickers hardness test uses a square-base diamond pyramid as the indenter. The included angle between opposite faces of the pyramid is 136°.

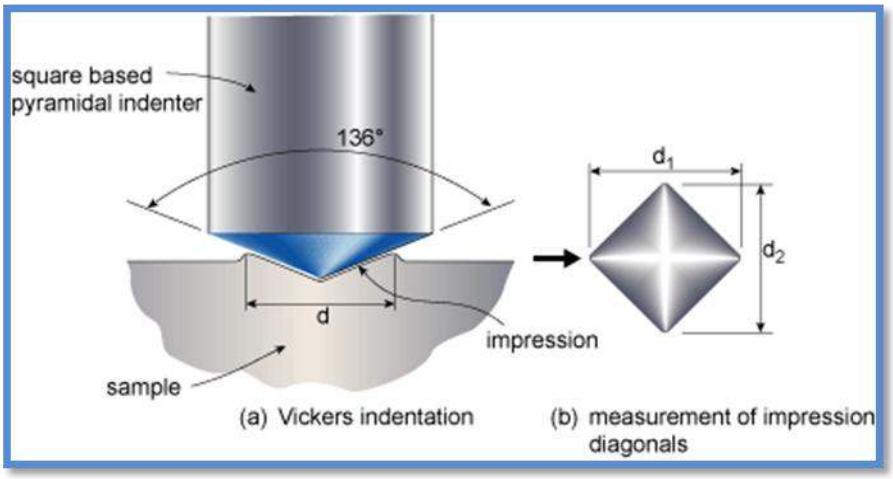

Figure 30. Vickers hardness test machine working principle [17].

Because of the shape of the indenter, this is frequently called the diamond-pyramid hardness test. The diamond-pyramid hardness number (DPH), or Vickers hardness number (VHN, or VPH), is defined as the load divided by the surface area of the indentation. In practice, this area is calculated from microscopic measurements of the lengths of the diagonals of the impression. The DPH may be determined from the following equation [17].

$$DPH = \frac{2\,P \sin(\theta/2)}{L^2} = \frac{1.854\,P}{L^2}$$

Where

P - Applied load, kg
L - average length of diagonals (d_1+d_2/2), mm
θ - angle between opposite faces of diamond = 136°

Different loads are applied on different hardness testing machines for example in vicker's micro hardness test machine we can measure from 10 to 1000 g and in our macro vicker's tester we can measure from 5 kg to 100 kg. The load is usually applied for 10 to 15 seconds.

The Vickers hardness test has received fairly wide acceptance for research work because it provides a continuous scale of hardness, for a given load, from very soft metals with a DPH of 5 to extremely hard materials with a DPH of 1,500 [17].

7 Results and Discussion:

In order to determine the fatigue resistance of steels by SCF, 60 tests were performed on the samples and the microstructures are shown in Figure 31.

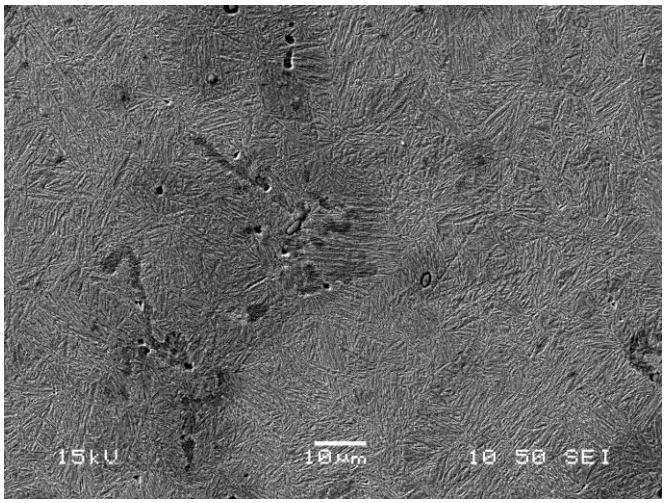

(a)

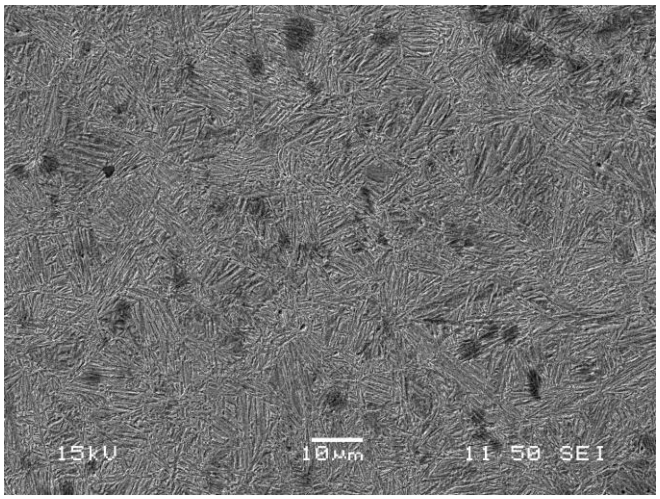

(b)

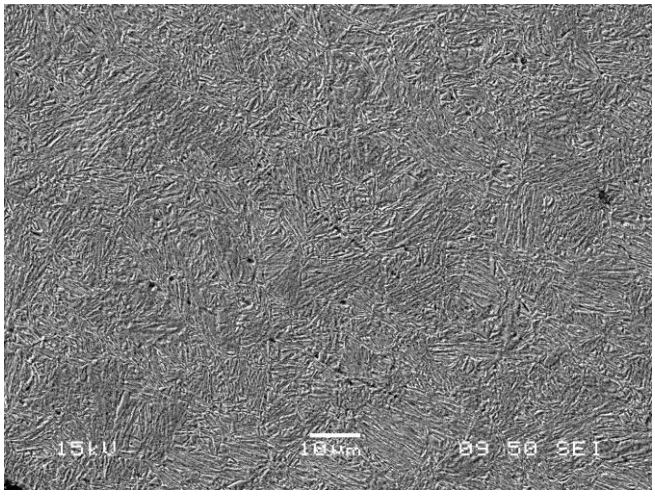

(c)

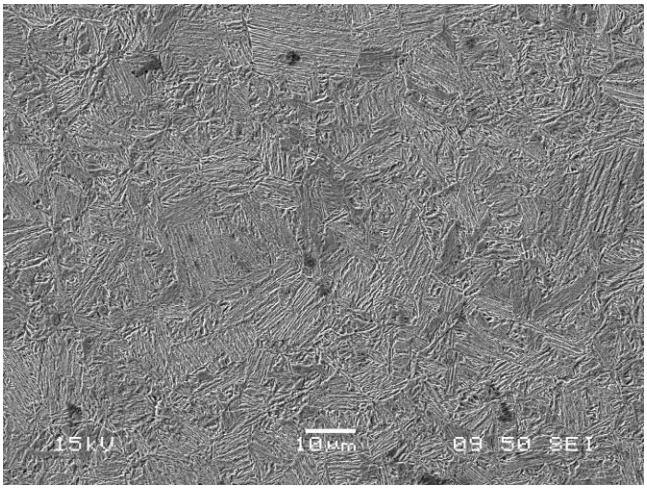

(d)

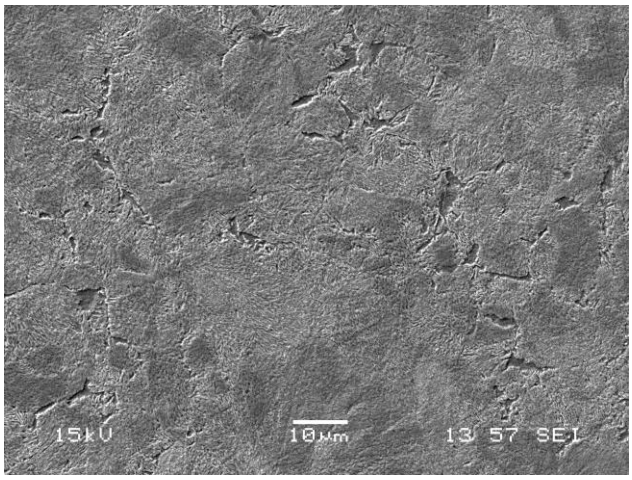

(e)

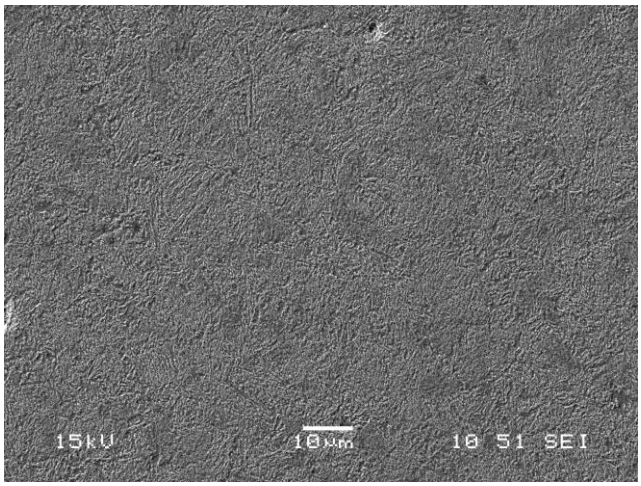

(f)

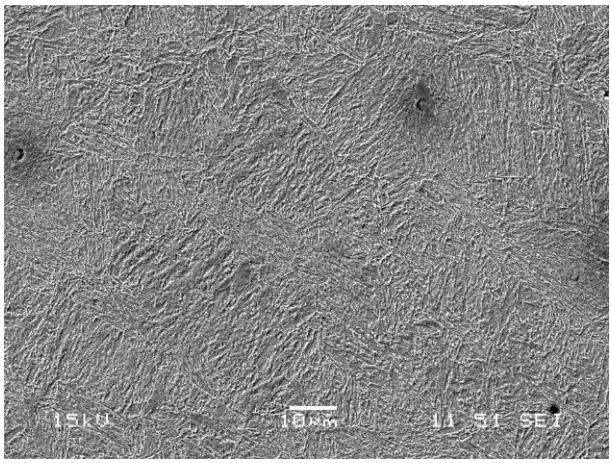

(g)

(h)

(i)

Figure31. SEM images showing ausferritic steels austempered at 250ºC, 275ºC, 300ºC, 350ºC (a-d), Pearlite, Lower bainite, Quench and tempered (SS 14 2244 steel) (e-g), Optical microscope images of Quench tempered (200 ºC, 1 hr) and fully Martensite specimens. 1000X (h-i).

The ausferritic steel austempered at 250 ºC having a hardness of 600 HV, has shown better fatigue limit (600000 cycles) than the results obtained for radial cracks (15 KN load) in the work done by Mathias Linz shown in Figure 33 of 300000 cycles and work done on air hardened steel by Fouad B. Abudaia [18] and [19].

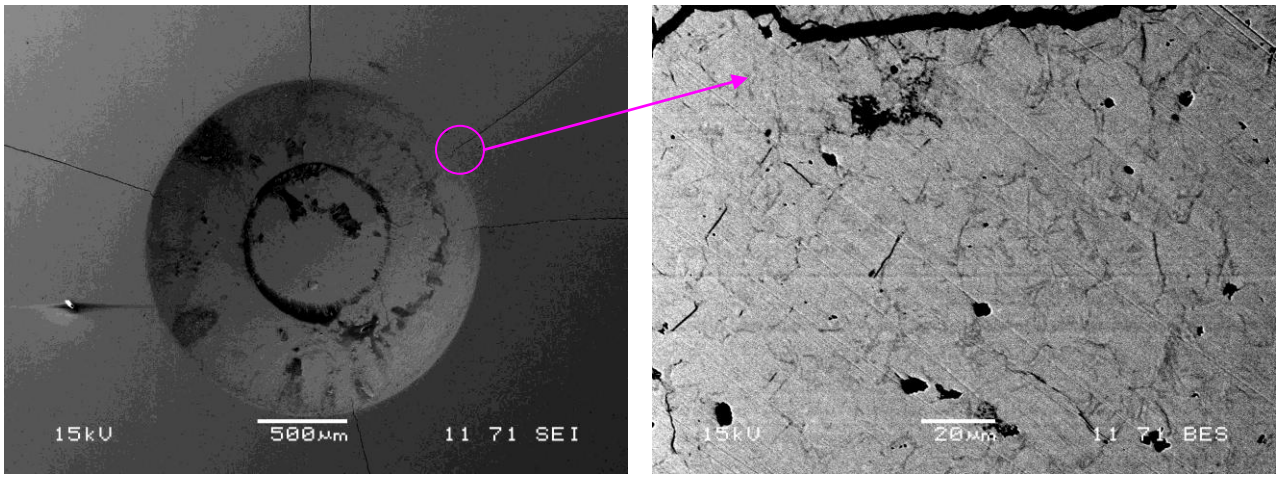

Figure 32. SEM image showing radial cracks after 6 00 000 cycles of ausferritic steel austempered at 250^0C.

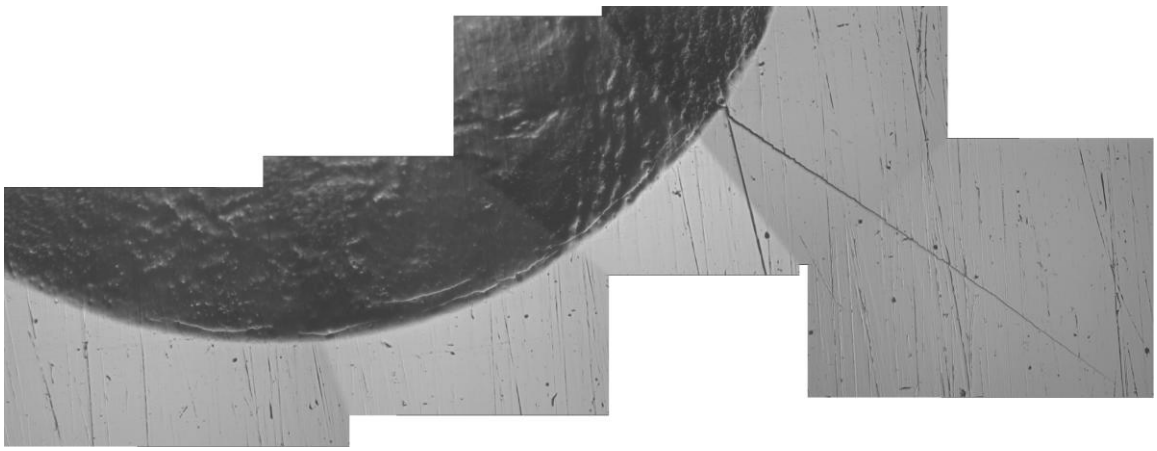

Figure 33. Radial cracks in the work done by Mathias Linz after 3 00 000 cycles [18].

Figure 34(b) shows the fatigue cycles required for different microstructures and explain that for Q + T (200 ºC, 1 hr) sample the cracks initiated very earlier than the ausferritic steel austempered at 275 ºC. Figure 35 shows the SEM images of radial cracks which has developed (at 15 KN load) due to plasticity at the load levels required for fatigue crack initiation.

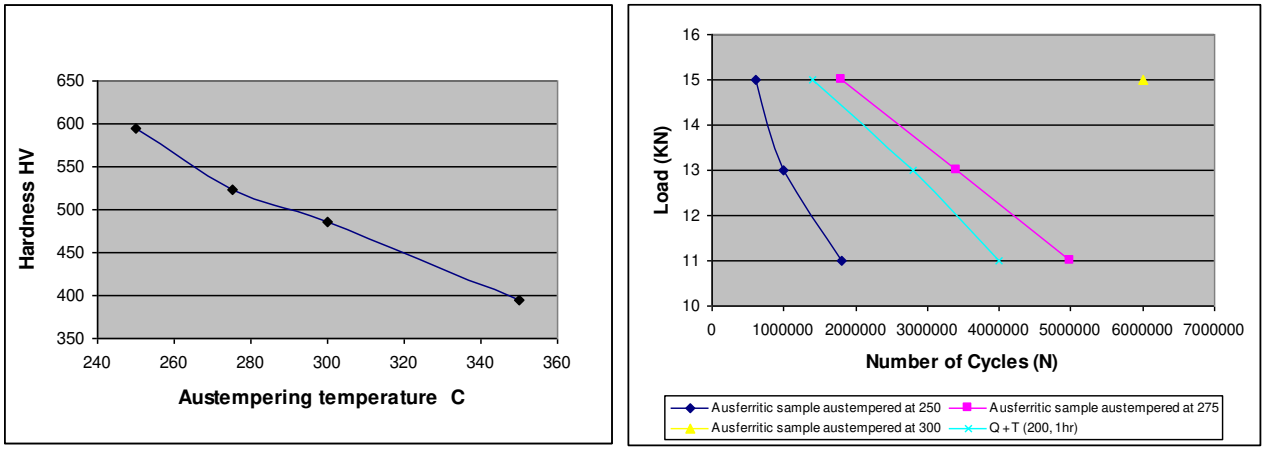

(a) *(b)*

Figure 34. (a) Hardness profile of ausferritic microstructure austempered at different temperatures.

(b) S – N Curve of different microstructures.

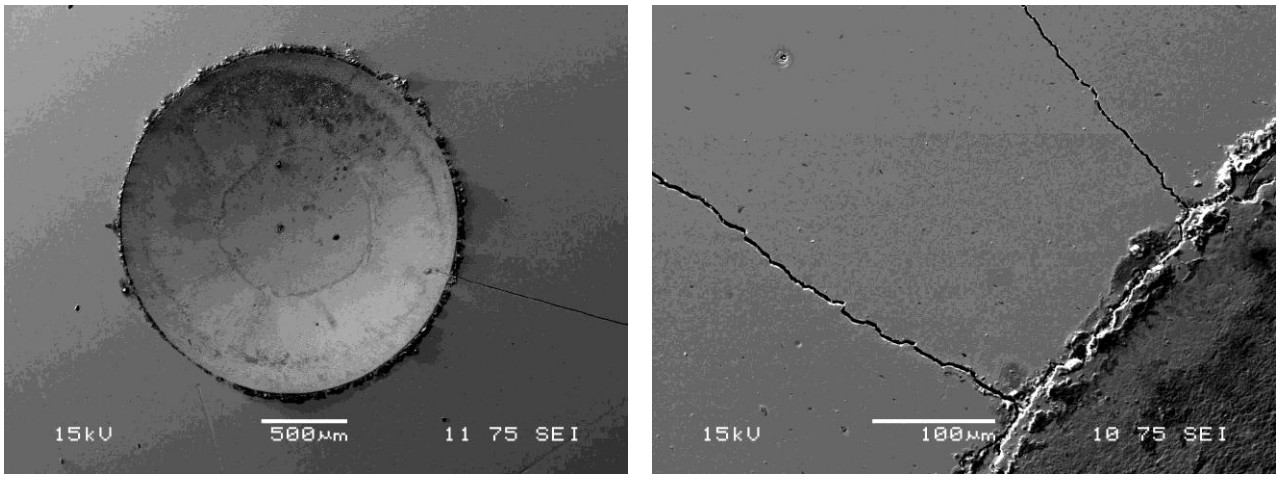

Figure 35. SEM images of ausferritic steel austempered at 275^{0}C & Quench and tempered (200 ºC, 1hr) specimen.

From the experimental results in Figure 36 and 37 it is known that for the ausferritic steel austempered at 300 ºC very small cracks were initiated after running 6 million cycles which is normally very high and this might be due to increase in retained austenite percentage(soft phase) of the material.

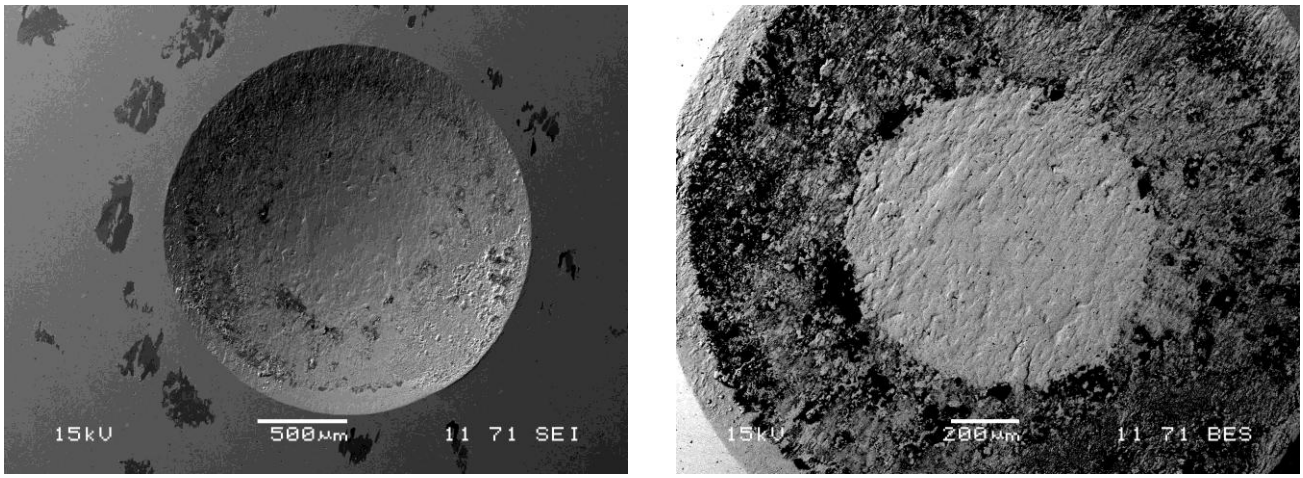

Figure 36. SEM images of ausferritic steel austempered at 300^{0}C after 18 00 000 cycles test.

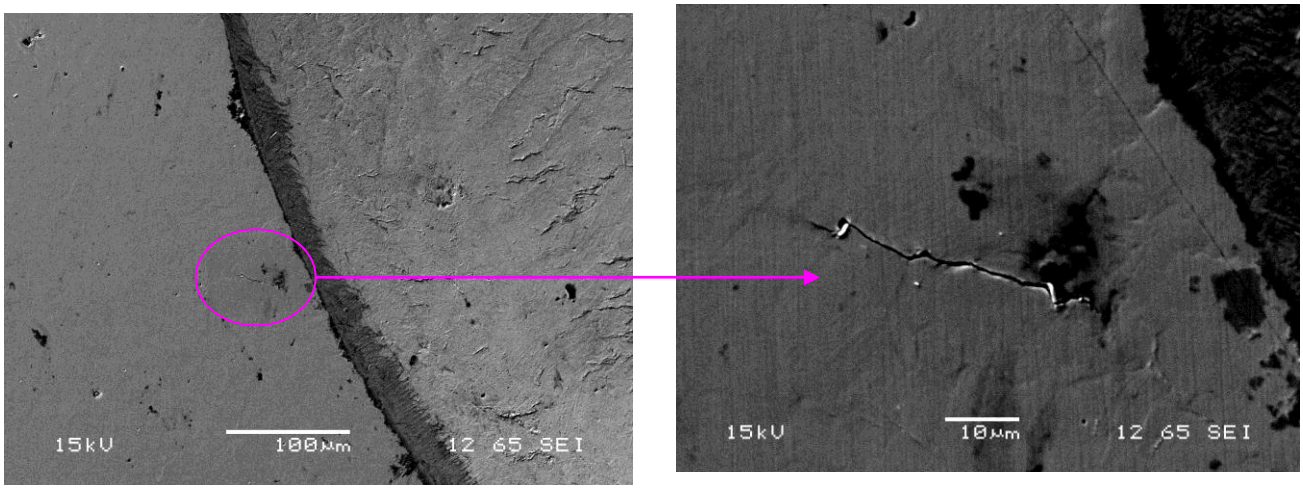

Figure 37. SEM images after 60 00 000 cycles of ausferritic steel austempered at 300^{0}C.

The X-ray diffraction analysis of the microstructures Figure 38 shows that with an increase in austempering temperature there is an gradual increase in retained austenite

percentage from 12.25 % to 17.80 % for 250 ℃ to 350 ℃ samples and decrease in hardness of the material.

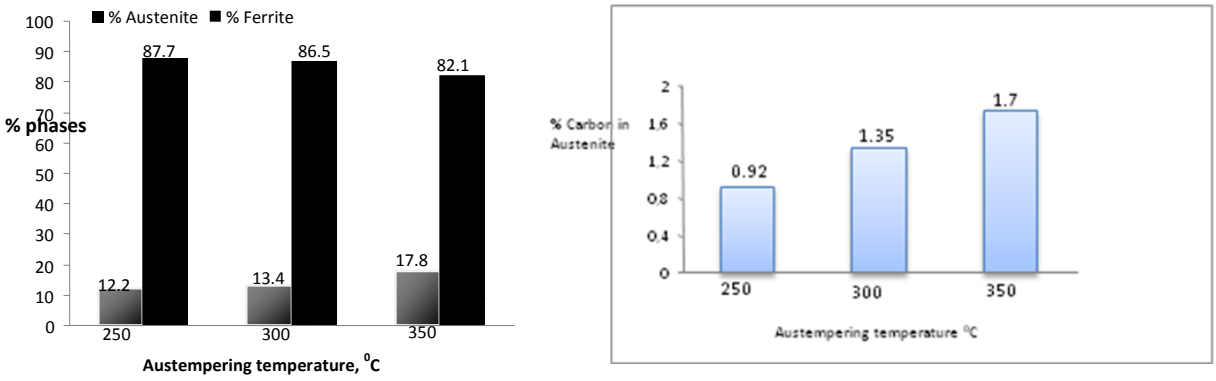

Figure 38 Volume fractions of retained austenite in ausferritic steels austempered at different temperatures & Carbon content in retained austenite.

A graph of intensities for different austempered temperatures and different peaks as a function of the diffraction angle 2θ is displayed, in Figure 39. From the above all mentioned comparison statements the result shows that the fatigue resistance of ausferritic steel is superior to the other microstructures in the work.

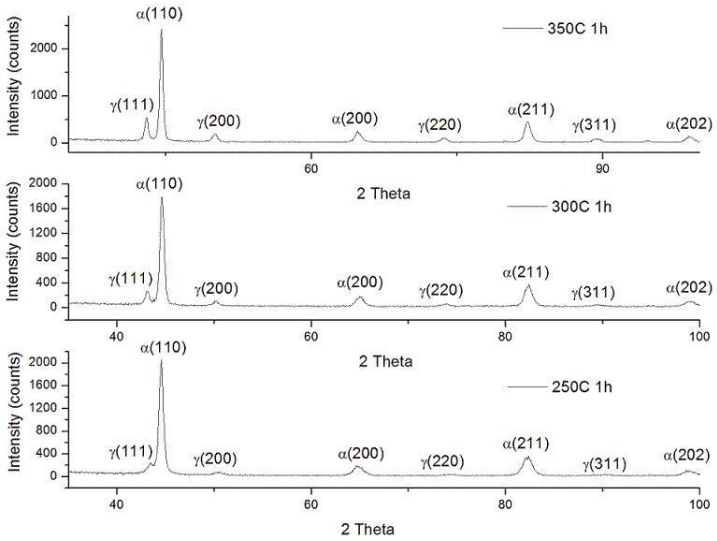

Figure 39. X-ray diffraction spectrum.

From Figure 40-43, it is evident that cracks are absent for the lower hardness and lower yield strength materials after running 1800000 cycles tested with 15 KN load.

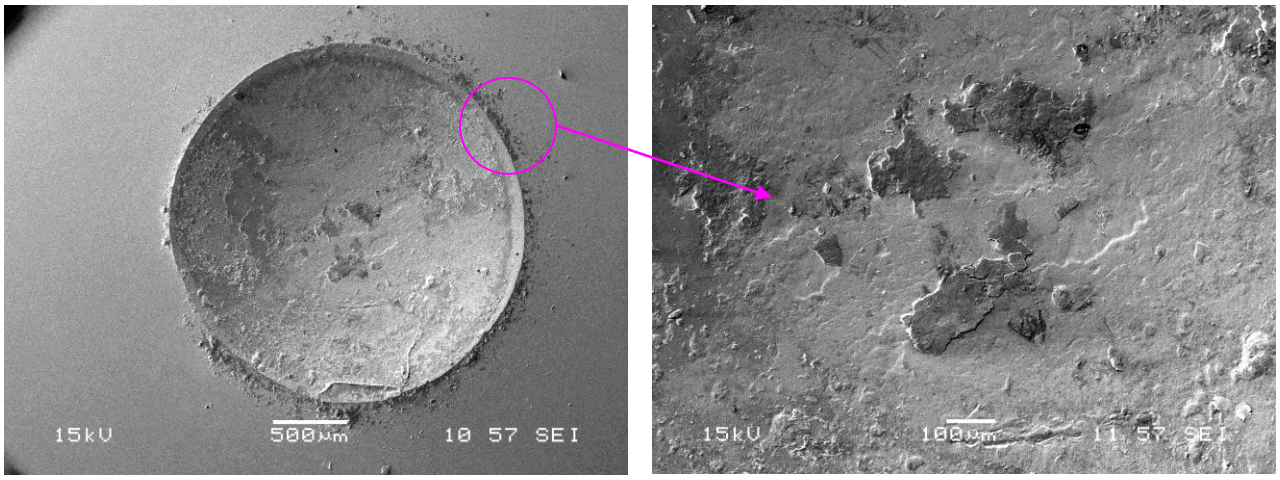

Figure 40. SEM images of ausferritic steels austempered at 350^{0}C, after 18 00 000 cycles and 15KN load

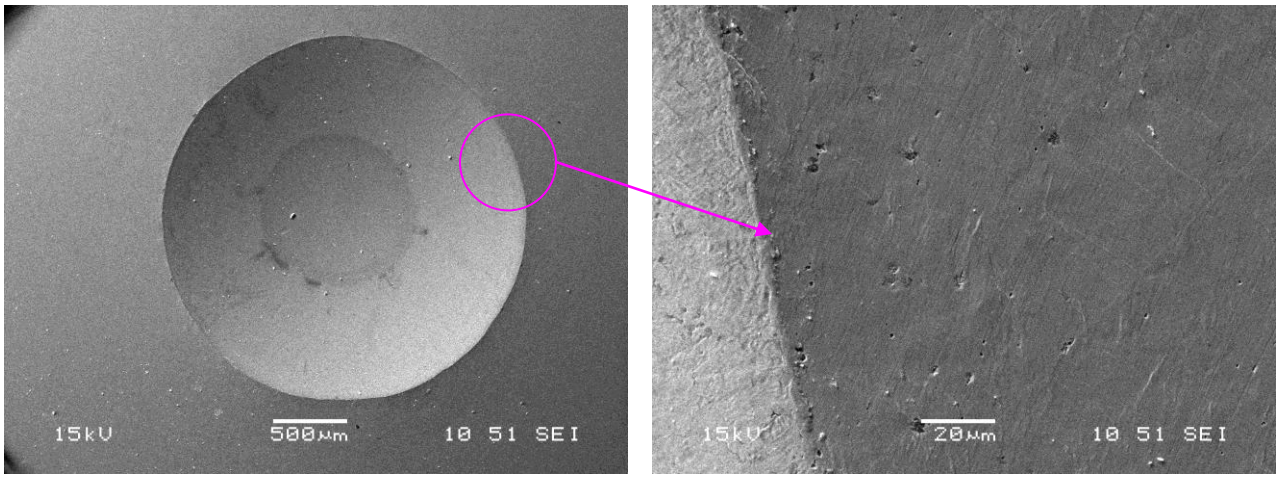

Figure 41. SEM images of lower bainitic steels, after 18 00 000 cycles and 15KN load.

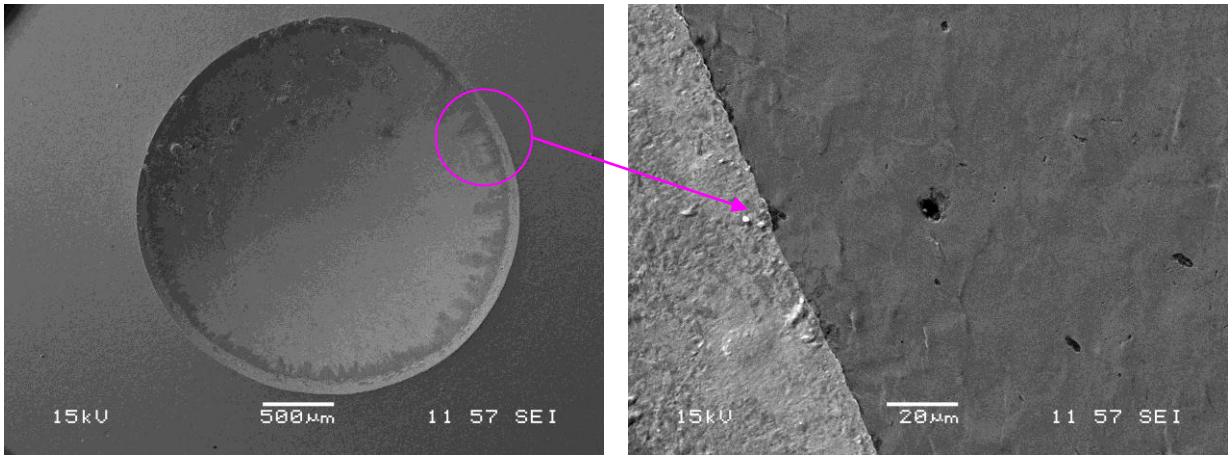

Figure 42. SEM images of pearlitic steels, after 18 00 000 cycles and 15KN load.

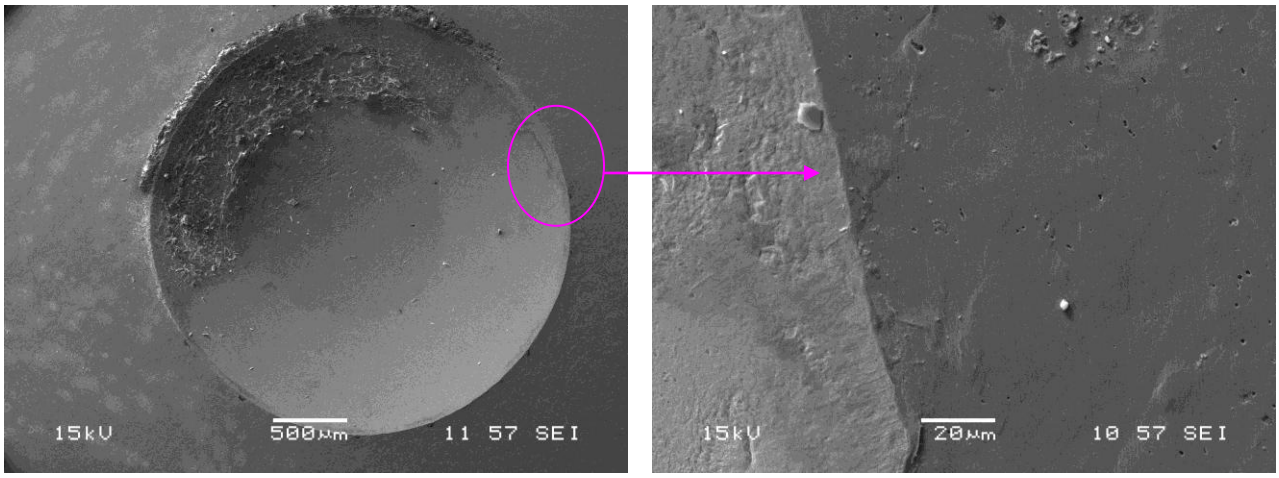

Figure 43. SEM images of Quench and tempered (2244) steel, after 18 00 000 cycles and 15KN load.

The reason behind this can be explained by the theory of contact stresses and the Goodman relation which tells about the importance of mean stress and states that the lifetime of a component working under fluctuating stress or cyclic loading is affected by the stress cycles. Therefore it is important to define the stress cycle in terms of the highest and lowest applied stress. The equation (1) explains the influence of mean stress and stress amplitude on fatigue failure criteria. [21]

$$\sigma_a = \sigma_{fat} * (1 - \sigma_m / \sigma_{ts}) \qquad (1)$$

Where

σ_a = Alternating stress or Fatigue strength,

σ_m = Mean stress,

σ_{fat} = Fatigue limit,

σ_{ts} = Ultimate tensile stress.

Theory of Contact stresses:

When the surfaces of the specimen and the indent are placed in contact they touch at one or few discrete points and if the surfaces are loaded, the contacts flatten elastically and the contact areas grow until failure of some sort occurs. The failure can be because of the compressive stresses, tensile fracture by tensile stresses or may be due to yielding caused by shear stresses.

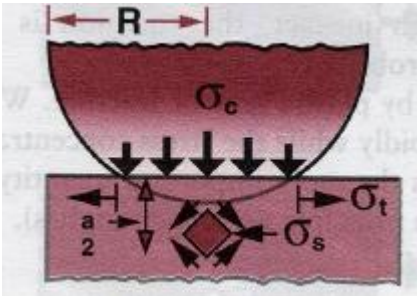

Figure 44. Contact stresses.

At low pressure or at lower loads the deformation is elastic and when the shear stresses exceed the shear yield strength a plastic deformation zone appears. With increasing the loads the plastic region connects with the surface forming fully plastic zone beneath the indent of the material. In the fully plastic state the mean pressure is expected to be 3 times that of yield strength for an elastic-perfectly plastic material (Johnson, 1985) [22].

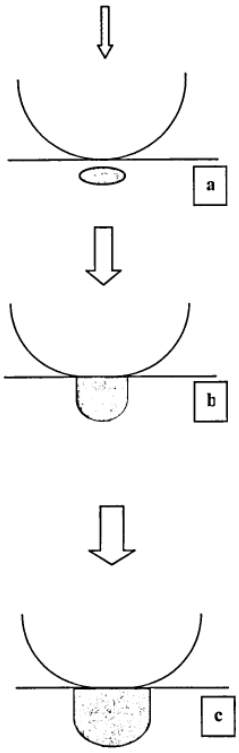

Figure 45. Stages in developing of a plastic zone [22].

The various stages in developing of plastic zones are

(A). Yielding commences below the surface.

(B). Elastic-plastic stage developed when plastic zone connects with the surface below the indenter.

(C).Fully plastic deformation occurs when plastic zone grew to connect with the free surface

The standing contact fatigue process is influenced by a large number of parameters e.g. contact load, relative slip, surface roughness, residual stresses, surface hardness, maximum compressive stresses, shear stresses and tensile stresses. The maximum stress values that are formed beneath the indent can be calculated by using the mentioned formulae. The material with high tensile stresses on the surfaces or near to the indent area formed by the SCF – test are more prone for initiation of cracks.

$$(\sigma_c)_{max} = 3F / 2\pi a^2 \qquad (2)$$

$$(\sigma_s)_{max} = F / 2\pi a^2 \qquad (3)$$

$$(\sigma_t)_{max} = F / 6\pi a^2 \qquad (4)$$

Where

σ_c = Compressive stresses, σ_s = Shear stresses,

σ_t = Tensile Stresses, F = Load (N),

a = Radius of contact (m).

The equation (2) (3) & (4) tells about the theory of contact stresses [22] and explains the types of stresses that can develop in the material due to application of cyclic load. The calculated stresses and hardness values shown in Table 3 explains that for the ausferritic microstructure a very high and very low stresses have been obtained. The importance of stresses around local surface asperities for contact fatigue is clearly described by Olsson in [10]. Thus the stresses developing in the material and the key role of yield strength in the material explain the reason why cracks didn't developed or developed very late in ausferritic and other microstructures.

Table3. Showing various parameters and its values for different microstructures.

The Tensile, compressive and shear stresses were calculated using the formulae mentioned in theory of contact stresses analysis for load of 15 KN (18 00 000 cycles).

Sno.	Structure	Hardness Values (HV)	Radius of contact ´a` (meters)	Tensile stresses (Mpa)	Compressive stresses (Mpa)	Shear stresses (Mpa)
1	Fully Pearlitic Steel	355	0.0014	406	3654	1218
2	Q & T Steel	336	0.0015	353	3183	1061
3	Lower Bainitic Steel	447	0.00125	509	4583	1527
4	Ausferritic Steel. Temp -1 250^0C	595	0.00095	881	7935	2645
5	Ausferritic Steel. Temp -1 275^0C	523	0.001	795	7161	2387
6	Temp – 2 300^0C	485	0.00105	721	6496	2165
7	Temp – 3 350^0C	394	0.00125	509	4583	1527
8	Q + T Steels (200, 1 hr)	532	0.001	795	7161	2387

Formation of oxides:

Oxides are usually named after the number of oxygen atoms in the oxide. Oxides are widely and abundantly distributed in nature e.g. water is the oxide of hydrogen. In this study electron backscatter diffraction in the SEM has been used to characterize the microstructure of oxide scales formed. It is expected that the oxides are mainly formed due to application of loads and due to contact area between specimen and the SCF test ball indenter.

Table 4. Chemical Composition of sample austempered at 300^0C.

Element	Weight%	Atomic%
O K	1.69	5.63
Si K	0.32	0.62
Cr K	0.49	0.50
Mn K	0.38	0.37
Fe K	97.12	92.88
Totals	100.00	

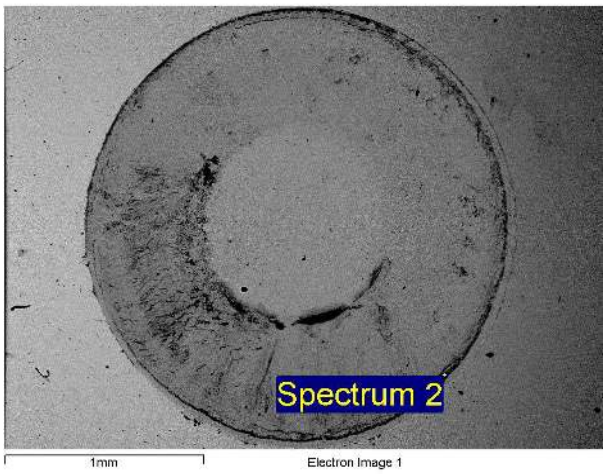

Figure 46. Area at which EDS performed for the ausferritic sample austempered at 300^0C.

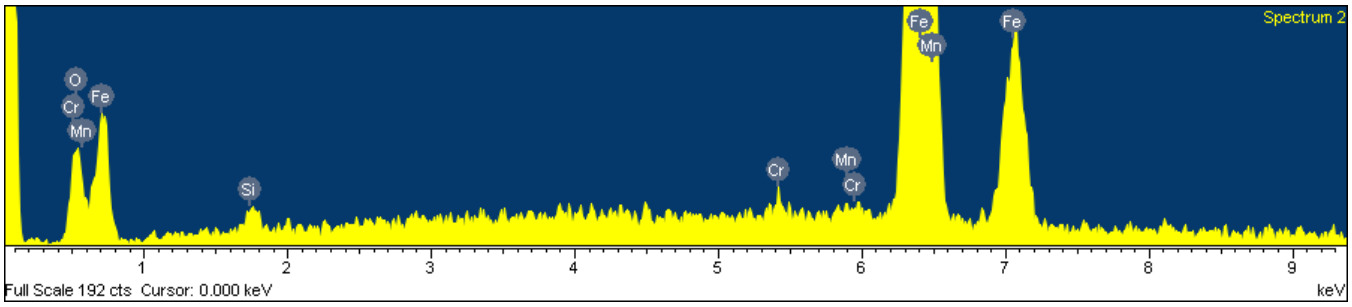

Figure 47.Spectrums for the ausferritic sample austempered at 300^0C.

Figure 47. Shows the dark area at which the EDS were performed. Iron-oxide was the most which formed in the material at spectrum – 2.

The EDS was performed at spectrum – 3 outside the indent of ausferritic sample austempered at 300^0C.

Table 5. Chemical Composition of sample austempered at 300^0C.

Element	Weight%	Atomic%
Si K	0.34	0.67
Cr K	0.29	0.31
Mn K	0.77	0.78
Fe K	98.61	98.24
Totals	100.00	

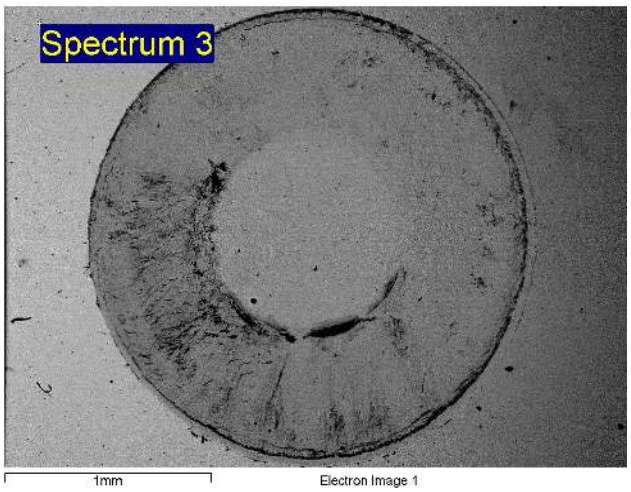

Figure 48. Area at which EDS performed.

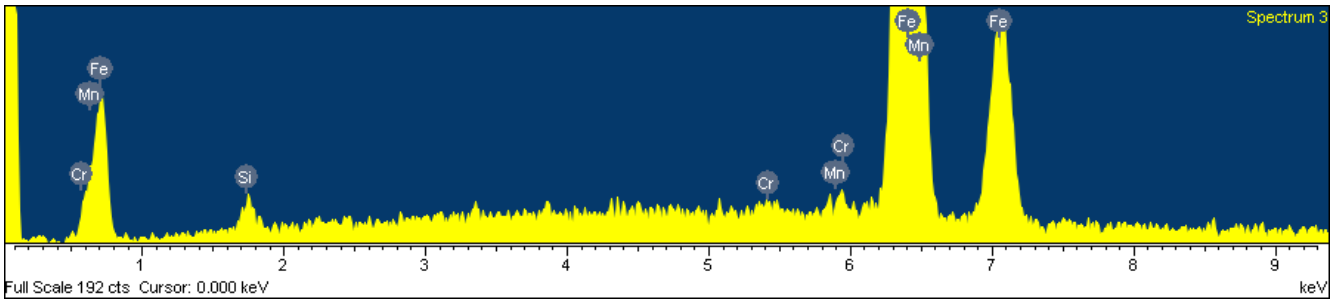

Figure 49. Spectrums – 3 for the Ausferritic sample Austempered at 300^0C.

Table 5 shows the chemical composition of the base material (ausferritic sample austempered at 300 0C). Table 4, 6 and 7 gives us the information about the percentage of iron oxides formed on ausferritic samples. Table 8 and 9 shows that very less percentage of iron oxide formed on samples compared to ausferritic sample. This might be due to loss of pure surface contact between the sample and ball indenter (in the machine holder).

Table 6. Chemical Composition of sample austempered at 275 ^{0}C.

Element	Weight%	Atomic%
O K	3.20	10.33
Cr K	0.49	0.49
Mn K	0.85	0.80
Fe K	95.47	88.38
Totals	100.00	

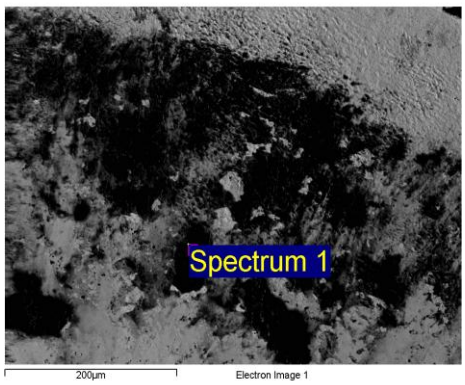

EDS performed for 2750C

Figure 50. EDS results for the Ausferritic sample Austempered at 275^{0}C.

.

Table 7. Chemical Composition of sample austempered at 350 ^{0}C.

Element	Weight%	Atomic%
O K	3.01	9.77
Si K	0.12	0.23
Cr K	0.15	0.15
Mn K	0.91	0.86
Fe K	95.80	88.99
Totals	100.00	

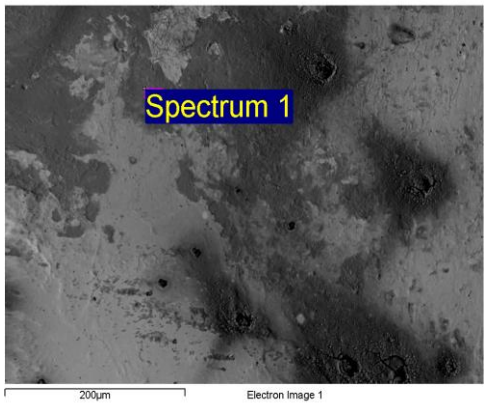

EDS performed for 350^{0}C

Figure 51. EDS results for the Ausferritic sample Austempered at350^{0}C.

Table8. Chemical Composition of sample with Quench and tempered (200 ºC, 1 hr).

Element	Weight%	Atomic%
O K	3.75	11.98
Mn K	1.11	1.04
Fe K	95.13	86.98
Totals	100.00	

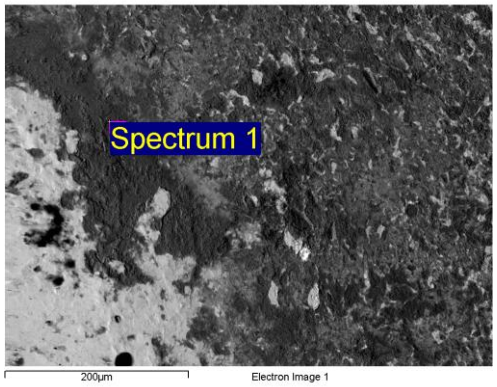

EDS performed for Q + T (200, 1 hr)

Figure 52. EDS results for the Quench and tempered (200 ºC, 1 hr) sample.

Table 9. Chemical Composition of sample with Lower bainite.

Element	Weight%	Atomic%
O K	1.06	3.60
Si K	0.32	0.63
Cr K	0.39	0.41
Mn K	0.78	0.77
Fe K	97.44	94.59
Totals	100.00	

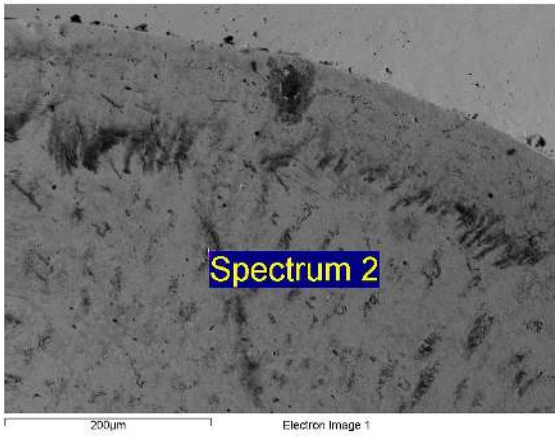

EDS performed for Lower Bainite

Figure 53. EDS results for the lower bainite.

8 Conclusions

The main aim of the thesis was to understand the contact fatigue resistance of one silicon containing steel using a Standing contact fatigue test machine (new approach), which can be treated in order to give it a carbide free bainitic microstructure and compare with other microstructures of steel.

The work was divided into three-main parts.

1. Production of different microstructure.
2. Testing on Standing Contact Fatigue (SCF) machine.
3. Characterization and analysis of the results obtained.

The objective of the thesis work was achieved. The SCF test analysis results turned out as an adequate method of testing different materials and also showed that chrome-steel balls are not suitable for testing samples with a high hardness (approx. 700 HV). The investigation of the different microstructures has shown that it is hard to distinguish a single criterion that well describes all aspects of the experimental results.

The number of cycles required for the crack to be initiated in ausferritic steels has clearly showed that the material has good strength and fatigue resistance properties. The surface hardness and the stresses developed in the material due to SCF test also had a clear influence on the fatigue damage generation.

The final results shows that the contact fatigue resistance of the ausferritic silicon steel was considerably better than that of the other microstructures in the work and there is no increase in bulk hardness of the material beneath the indent and no sub-surface crack could be detected.

9 Future work

A number of standing contact fatigue test experiments was performed on the steel material. But for better analysis of the material it would be interesting to continue with the following investigations

- Performing 180 00 000 cycles SCF-test with 15 KN load on ausferritic steel austempered at 350 ℃.
- Performing tensile tests for all ausferritic samples.
- Studying the effect of residual stresses on the standing contact fatigue resistance.

References:

1. ASM Handbook Volume 19, Published: 1996, Fatigue And Fracture
2. Tallian TE. Failure atlas for hertz contact machine elements. New York: ASME Press, 1992.
3. Hoo JJ, editor. Rolling contact fatigue testing of bearing steels. Philadelphia: American Society for Testing and Materials, 1982 ASTM STP 771.
4. Bold, P. E., Brown, M. W., Allen, R. J., "Shear Mode Crack Growth and Rolling Contact Fatigue", Wear, vol. 144, pp. 307–317, 1991
5. http://www.ndt-ed.org.
6. http://www.engrasp.com/doc/etb/mod/fm1/stresslife/stresslife_help.html.
7. Alfredsson B, Olsson M. Standing contact fatigue testing of a ductile material: surface and sub-surface cracks. Fatigue and Fracture of Engineering Materials and Structures 1999.
8. Olsson M. Contact fatigue and tensile stresses. In: Beynon JH, Brown MW, Lindley TC, Smith RA, Tomkins B, editors. Engineering against fatigue. The Netherlands: AA Balkema, 1999.
9. Mattias Widmark, Arne Melander. Effect of material, heat treatment, grinding and shot peening on contact fatigue life of carburized steels.
10. Alfredsson B, Olsson M. Standing contact fatigue of engineering materials and structures. Fatigue and Fracture 1999.
11. Alfredsson B, Olsson M. Initiation and growth of standing contact fatigue cracks.
12. http://www.materialsengineer.com/E-Steel%20Properties%20Overview.htm.
13. http://www.industrialheating.com.
14. www.cashenblades.com.
15. http://upload.wikimedia.org/wikipedia/commons/6/6b/Austempering.jpg
16. S.K. Putatunda, L. Bartosiewicz, F.A. Alberts and I. Singh, Influence of microstructure on high cycle fatigue behavior of austempered ductile cast iron. Mater Charact 30 (1993), pp. 221–234.
17. http://www.twi.co.uk/content/jk74.html

18. Contact fatigue testing of Cam ring steel. M.P. Linz. Master´s thesis 2010:005 PB ISSN:1653-0187

19. Master thesis work of Fouad B. Abudaia on Microstructure and Fatigue Strength of High Performance Gear Steels, New Castle University. United kingdom

20. Olsson M. Contact fatigue and tensile stresses. In: Beynon JH, Brown MW, Lindley TC, Smith RA, Tomkins B, editors. Engineering against fatigue, 1997 Mar. 17–21; Sheffield (UK). Rotterdam: A.A. Balkema, 1999.

21. Hertzberg, Richard W. Deformation and Fracture Mechanics and Engineering Materials. John Wiley and Sons, Hoboken, NJ: 1996.

22. Material selection in mechanical design, 3rd edition, M.F Ashley Elsevier, 2005.

Appendix 1. Total number of experiments (SCF tests) performed.

Specimen	Cycles(N)	Load (KN)	Cracks
Ausferritic sample austempered at 250 ºC	100000		
	200000		
	500000		
	600000	15	Yes
	900000		
	1000000	13	Yes
	1500000		
	1800000	11	Yes
Ausferritic sample austempered at 275 ºC	400000		
	600000		
	1000000		
	1200000		
	1500000		
	1800000	15	Yes
	2500000		
	3400000	13	Yes
	3600000		
	4500000		
	5000000	11	Yes
Ausferritic sample austempered at 300 ºC	400000		
	800000		
	1500000		
	1800000		
	3000000		
	4000000		
	5000000		
	6000000	15	Yes
Ausferritic sample austempered at 350 ºC	1000000		
	1500000		
	1800000		
	2500000		
	4000000		
	5000000		
	6000000		
	7000000		

Specimen	Cycles(N)	Load (KN)	Cracks
Pearlitic	100000		
	500000		
	800000		
	1200000		
	1500000		
	1800000		
Q + T(2244)	100000		
	500000		
	800000		
	1200000		
	1500000		
	1800000		
Fully martensite	15 000		
	30 000	15	Yes
Lower bainite	100000		
	500000		
	800000		
	1200000		
	1500000		
	1800000		
Q + T (200 ºC , 1 hr)	300000		
	600000		
	1200000		
	1400000	15	Yes
	2000000		
	2800000	13	Yes
	3500000		
	4000000	11	Yes
	4500000		